This is to certify that the

thesis entitled

Photoelectrochemical, Electrochemical and Surface Analysis Studies of Rhodamine B, Erythrosin, and Various Other Dyes at Tin Oxide Electrode Surfaces presented by

David Dean Hawn

has been accepted towards fulfillment
of the requirements for

M.S. degree in Chemistry

Major professor

Date 11-8-77

O-7639

PHOTOELECTROCHEMICAL, ELECTROCHEMICAL AND SURFACE ANALYSIS STUDIES OF RHODAMINE B, ERYTHROSIN, AND VARIOUS OTHER DYES AT TIN OXIDE ELECTRODE SURFACES

by

David Dean Hawn

A THESIS

Submitted to

Michigan State University
in partial fulfillment of the requirements
for the degree of

MASTER OF SCIENCE

Department of Chemistry

1977

ABSTRACT

PHOTOELECTROCHEMICAL, ELECTROCHEMICAL AND SURFACE ANALYSIS STUDIES OF RHODAMINE B, ERYTHROSIN, AND VARIOUS OTHER DYES AT TIN OXIDE ELECTRODE SURFACES

By

David Dean Hawn

The modification of semiconductive electrodes in order to enhance their photocurrent-producing abilities has been of recent interest. Because of the relatively large band-gaps of these semiconductors (3.0-3.5 volts), their current producing abilities are rather poor under illumination with visible light. However, modification of these materials with suitable dye materials, which absorb light in the visible regions and have high molar absorptions, can greatly increase the semiconductor's photoefficiency.

In order to investigate this phenomenon, we have examined both multilayer dye configurations constructed electrochemically and monolayer dye assemblies constructed covalently.

For characterization of these surfaces using surface-sensitive spectroscopic techniques, such as ESCA, we have resorted to the use of various tagged dye molecules. Because most dye molecules used to date have contained only carbon, nitrogen and oxygen atoms, ESCA analysis of these

materials is of little interest, since these atoms are also present as contaminants on the surface. However, the use of halogenated dyes has allowed us to unambiguously quantitate the dye concentrations on the modified electrode. Results from this surface spectroscopic technique have led us to believe that electrochemical adsorption of erythrosin dye at silane-modified surfaces produces more than one form of surface bound dye.

For covalent attachment, two procedures have been investigated. One is an amidization reaction, between the carboxylic acid group of the dye, and an amine group on the electrode surface, in the presence of dicyclohexylcarbodiimide. The other involves the formation of a thiol linkage between a mercapto group on the surface of the electrode and the iodine substituents of the dye erythrosin.

Various electrochemical techniques have been employed to characterize electrodes modified in this manner, as well as the photocurrent producing abilities of both monolayer and multilayer assemblies. Final results have led us to believe that the covalent linkage plays more than a passive role in photocurrent sensitization. Covalent attachment does more than immobilize the dye on the surface. Photocurrents at electrodes with low concentrations of covalent attached dye consistently exceed photocurrents at electrodes with several layers of adsorbed dye.

ACKNOWLEDGMENTS

I thank my wife, Patti, for her help and patience in preparing this manuscript. I also thank my Mom and Dad for their encouragement through the years.

I also acknowledge Dr. Neal Armstrong, Dr. Lynn Sousa, and Dr. Michael Weaver for their many hours of helpful discussion.

For her technical assistance in preparing this manuscript, I wish to thank Dianne Contos.

TABLE OF CONTENTS

LIST OF TABLES

LIST OF FIGURES

CHAPTER I

HISTORY

A. Introduction

There has recently been great interest in the investigation of nonconventional forms of energy, the most important of which are nuclear and solar energy. Unfortunately, public awareness of the degradation of the environment has branded nuclear power a bad risk.

The sun, on the other hand, is one of the most promising alternative energy sources. It offers considerable amounts of power in the form of heat and light at an extremely low cost. Unlike nuclear power, there are no problems with solid waste disposal. There is no risk to health from radiation, and no fission processes to control. Solar energy is not without its problems, however. The biggest of these is the conversion of radiation into some more useable form, such as electricity. Green plants, for example, take light and carbon dioxide and, with the aid of cholorphyll, convert light to food and water. Maybe we can borrow some technology from the plants to overcome this problem.

One such method of conversion is the solid-state silicon solar cell, which utilizes the energy of the sun to produce an electrical current. Another involves the generation of electrical currents using a semiconductor electrode, at an electrode-electrolyte interface. Such photovoltaic processes, commonly called Becquerel effects after their discoverer, offer an added advantage over strictly solid-state devices, however. When photocurrents are produced by the action of light at these electrode surfaces, it must be at the expense

of something at the electrode, or in the electrolyte, i.e., electrons. At the semiconductor electrode-electrolyte interface, the oxidation of water to produce molecular oxygen is a known phenomenon. This reaction is associated with anodic processes. In a similar fashion, cathodic processes can be used in the production of hydrogen by the reduction of water. Therefore, photovoltaic processes can also result in the production of combustible fuels.

Many investigators have observed photoeffects at various semiconductor electrode materials, such as titanium dioxide (TiO_2) (1), zinc dioxide (ZnO_2) (2,3) and tin dioxide (SnO_2) (4). It is generally observed that illumination of the semiconductors with radiation of bandgap energy produces electron-hole pairs which can participate in electrochemical processes. For example, at p-type semiconductors, electrons for cathodic photocurrents result, while at n-type materials, such as those listed above, holes, and anodic photocurrents result. Tin oxide, which has a bandgap of about 3.5 volts, will absorb light at about 300 nanometers or lower, generating current flow. Titanium dioxide, on the other hand, with a bandgap of about 3.05 volts, absorbs light around 380 nm. The fact that both of these materials have such a large bandgap makes them impractical as photoelectrochemical conversion devices.

Sensitization or enhancement of photocurrents can be accomplished if the electrode material is placed in contact with a suitable dye material, either adsorbed to the electrode

surface or placed in the electrolyte. This observation has generated many investigations since it was initially observed by Memming and Kursten (5). In this instance, illumination of the electrode-electrolyte interface with light absorbed by the dye only is sufficient to generate current flow.

Figure 1 summarizes this dye sensitization process, for metals, and both n-type and p-type semiconductors.

For a metal electrode, photocurrents can hardly occur, owing to the high density of occupied states in the metal. In this case, both the ground state S_0 of the dye, and the lowest excited state S_1 overlap with occupied energy bands in the metal, resulting in a two-step process which does no more than quench the excited dye molecule.

A completely different situation results in the case of semiconductors, however. The existence of a bandgap, or forbidden region, between the conduction band and the valence band permits a one-step process to occur, since it requires a finite time for recombination of holes and electrons within the semiconductor. Since an electron in the conduction band must traverse the forbidden region to reestablish electroneutrality in the semiconductor, it can only do so by passing through an external circuit, doing work in the process. If either the ground state S_0, or the excited state S_1 of the dye falls within the forbidden region of the semiconductor, no recombination step can occur after the oxidation or reduction of the dye, and a photocurrent should result. This requires that the bandgap of the dye is less than the bandgap

of the semiconductor. Photochemical sensitization is indeed the observed behavior for these types of electrodes. The utilization of this effect to increase photocurrents has been the entire object of this research. The use of various dye materials, either adsorbed or covalently attached, will be of significance in further energy research (6,7).

B. Electrode Preparation and Characterization

The principle substrate used in this research is chemically vapor-deposited polycrystalline tin oxide. During recent years SnO_2 electrodes have been frequently employed as optically transparent electrodes, or OTEs, for the spectrophotometric study of chemical reactions at electrode-electrolyte interfaces (8,9). SnO_2 layers on glass or quartz substrates show excellent optical transparency in the visible wavelength region, as well as high electrical conductivity.

Most tin oxide surfaces are prepared, either privately or commercially, by pyrolytic oxidation of various organo-tin compounds. The normal preparative procedure is to mix tin tetrachloride ($SnCl_4$) or tetrabutyl tin with a volatile solvent such as hexane or butylacetate. This mixture is atomized with nitrogen or oxygen and the vapors blown onto a substrate heated to 450 to 600^{o} C. Since pure tin oxide is an insulator, the conductivity can be widely varied by adding a dopant material, most commonly antimony or fluoride ion, rendering the material an n-type semiconductor. Layers ranging from 1000 to 5000 Angstroms thick are normally deposited on the substrate.

The physical and chemical properties of tin oxide have been studied in detail (10,11), as well as the surface characteristics (12).

Tin oxide is normally characterized by two parameters, its flat band potential and its carrier density. The flat band potential is the applied potential at which no banding occurs in the space charge region (62). The carrier density, which is related to the number of dopant molecules present, represents the number of majority carriers. In the case of tin oxide, the majority carriers are electrons, so that this material is an n-type semiconductor. Both of the above parameters can be determined by experimental measurement of the electrode capacitance as a function of applied potential, as outlined by Gileadi and others (13,14,15). The electrode capacitance, as measured in contact with an electrolyte, results from two major contributions, the Helmholtz capacitance (C_H) from the solution and the space charge capacitance (C_{SC}) from the semiconductor. These two capacitances act in series, so that the total capacitance, C, can be expressed as

$$1/C = 1/C_H + 1/C_{SC}$$

Investigations with other semiconductors have shown that differences in electrode potential lead primarily to changes in the potential drop across the space charge region. Therefore, in most cases, the total capacitance is essentially determined by the space charge value only, so that

$$1/C = 1/C_{SC}.$$

Calculation of the carrier density, n_o, using Poisson's equation (14) gives rise to an equation of the form

$$1/C^2 = 2/\varepsilon\varepsilon_o n_o)(U - U_{fb} - kT/e)$$

Here, ε and ε_o are dielectric constants of the tin oxide and of vacuum, e is the charge on an electron, and k is Boltzmann constant. U is the applied potential. The unknown parameters in this equation, n_o and the flat band potential U_{fb}, can be calculated from a plot of $1/C^2$ against the applied bias U, commonly called a Mott-Schottky plot. Inspection of the above equation reveals that the slope of the plot is inversely proportional to the carrier density, while at the x-intercept, where $1/C^2 = 0$, U equals U_{fb}, with a small correction term. The flat band potential U_{fb} is a particularly important parameter, since it is the applied potential at which no band bending occurs within the space charge region of the semiconductor. Provided the carrier density of the semiconductor is high, it is reasonably safe to assume that the fermi level and the conduction band of the semiconductor are within 0.1 volts of each other (62). Carrier densities for polycrystalline tin oxide are normally in the range of 10^{19} to 10^{21} carriers/cm^3, with a flat band potential of approximately -1.0 volts as measured against a silver/silver chloride reference (15).

The surface of SnO_2 is made up primarily of amphoteric Sn-OH groups. The solution pH can influence the degree of dissociation of these groups according to the relations

$$Sn\text{-}OH \rightleftharpoons Sn\text{-}O^- + H^+$$

or

$$Sn\text{-}OH \rightleftharpoons Sn^+ + OH^-$$

Thus, the solution pH can have a large effect on the flat band potential, due to variations in potential drop across the Helmholtz plane, but should have no effect on the carrier density (16).

Linear sweep voltammetric studies of SnO_2 surfaces show three regions of electrochemical interest as shown in Figure 2 (17). In aqueous solutions, SnO_2 electrodes show a large rise in current production at potentials of 1.2-1.4 volts anodic, as measured against a silver/silver chloride reference. In this region oxygen evolution occurs due to the oxidation of water. At the opposite end, at potentials of -0.2 to -0.5 volts, the reduction of water and the evolution of hydrogen gas is observed. Although brief excursions to and beyond the anodic limit do not disrupt the tin oxide surface in any way, potentials beyond the cathodic limit result in destruction of the conductive layer, which is reduced to metallic tin (17).

In the intermediate region, only slight current passage is observed, due to charging and discharging of the surface space charge region. The quality of the tin oxide and the solution pH strongly affect the magnitude of charging current and the location of both the anodic and cathodic limits.

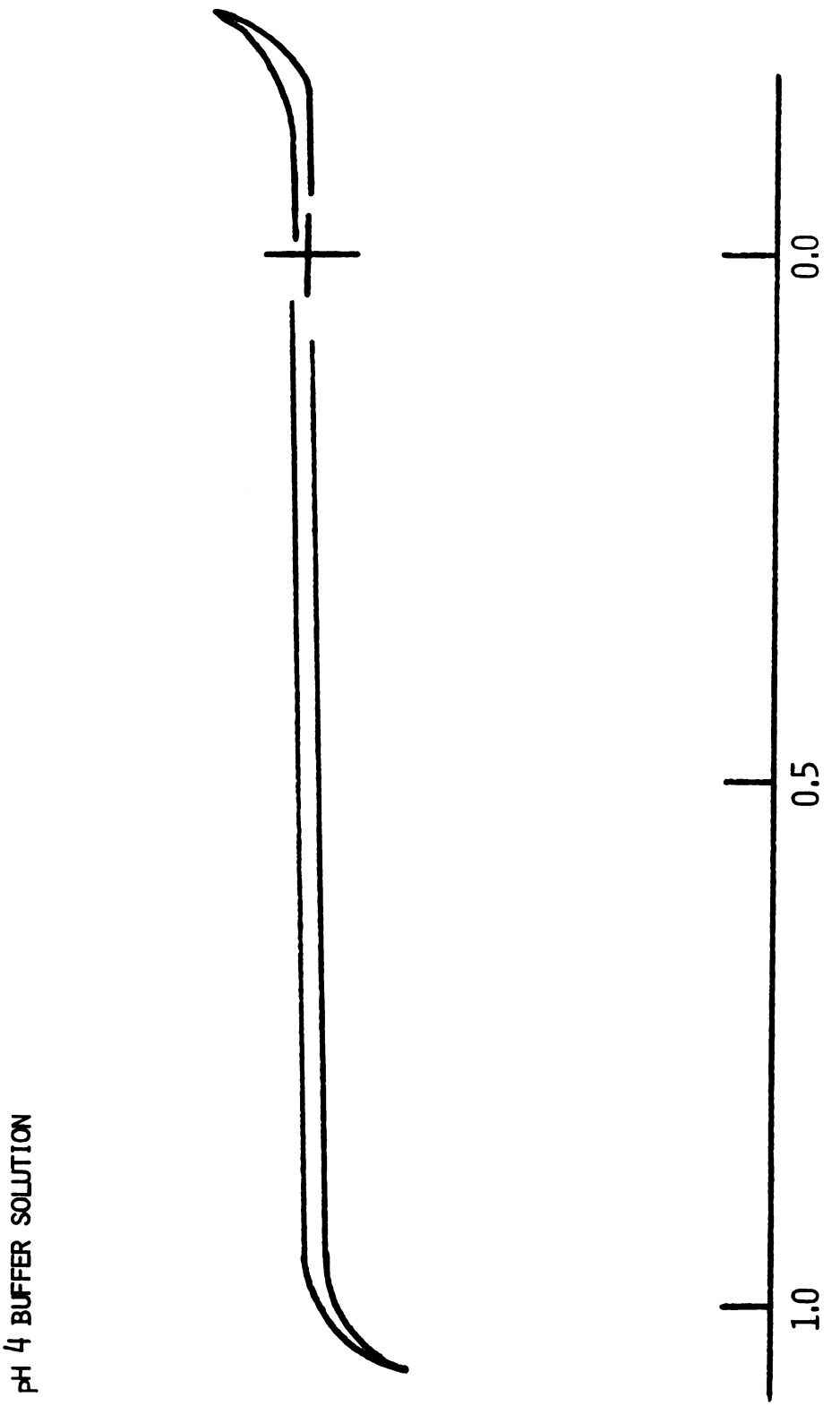

Figure 2. Cyclic voltammagram of pH 4 buffer at clean tin oxide electrode; scan rate = 11.5 mv/sec.

C. Silane Modification

The silanization of surface-active materials in order to alter their physical or chemical properties is widely known. Silanes are that class of compounds which consist of a silicon atom at the center, attached to four organic groups of various functionality. Most commonly, silanes are used to modify surfaces of silica chromatrographic supports, such as Zipacs or diatomaceous earths, in order to improve their behavior as stationary phases. These silica supports, their chemical modification, and chromatographic performance have received great attention in the literature.

Various references in the area of both gas chromatography and liquid chromatography have discussed the silane modification of solid supports to improve their chromatographic properties (18,19,20). An excellent review of these stationary phases, and their use as chromatographic columns has been published by Locke (21).

The use of silanes for the chemical modification of semiconductor surfaces, however, has only recently been of interest. The wide variety of these silicon-based materials, in terms of availability as various organofuctional derivatives (23), have made them attractive for intermediates for covalent attachment to these surfaces. Further, their highly reactive nature, especially with oxide-type surfaces, and excellent thermal and chemical stability, make them attractive choices for modification.

The reaction of an organosilane reagent with a surface hydroxyl group, such as tin oxide or titanium dioxide, can be represented by the following reaction (24):

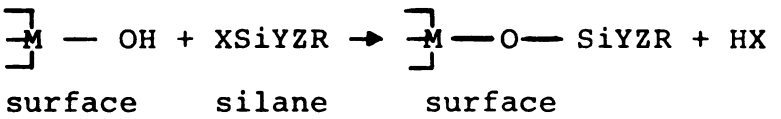

Treatment of these derivatized surfaces with concentrated nitric or hydrochloric acids at room temperature have little effect on the surface. Over long periods of time, however, hydrolysis of the surface groups is observed, with the subsequent removal of bonded silane material (24).

The known order of reactivity of organosilanes with silica surfaces, such as those used in chromatography, is $X_3SiR > X_2SiR > XSiR_3$ (25). Most commonly, the reactive leaving groups (X) are chloride (Cl), methoxy (MeO), or ethoxy (EtO). For a given silane reagent, reactivity with a surface increases in the series X=Cl > X=MeO > X=EtO.

Organosilanes with more than one reactive group (X) have the possibility of binding to the surface at more than one site. This does not necessarily mean that silanes with two reactive groups must bind at two sites, however. The fate of the remaining unbonded reactive groups is also of some importance, especially in the formation of stable conductive surface-bound phases. Polymeric formation can occur at the surface in the presence of water (20,26), forming a nonconductive surface layer of the form

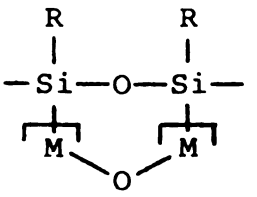

Polymerization can be avoided by the exclusion of water during attachment procedures or by the use of silanes with only one reactive group.

The reaction of methylchlorosilanes, either trimethylchlorosilane or dimethyldichlorosilane, with tin oxide gels, have been investigated by Harrison and Thornton, using infrared spectrometry (27, 28). It was observed that tin oxide discs which had been evacuated by 320 K showed an intense band due O-H stretching at 3600-2000 cm^{-1}. After reaction with a silane, however, the O-H band intensity decreased drastically. The mechanical properties of tin oxide gels so reacted also changed greatly, due to the reduction of interparticle hydrogen bonding. The most drastic changes occurred using dimethyl dichlorosilane, where the discs became extremely brittle.

The electrochemical behavior of SnO_2 electrodes modified with various silanes has been studied by Murray (29,35). Replacement of surface hydroxyl groups (Sn-OH) with silane groups showed little effect on the cyclic voltammetric behavior, although the magnitude of the charging current was reduced in the silane-modified case. Cyclic voltammetric behavior toward the electrochemically reversible couple ferri/ferrocyanide were also unchanged between the clean and

silane-modified tin oxide surfaces. The authors did notice a slight increase in the peak potential separation of the (Fe^{2+}/Fe^{3+}) oxidation and the (Fe^{3+}/Fe^{2+}) reduction after the surface had been modified, indicating a slight reduction in the accessibility of the reactants to the electrode surface.

Murray (64) has attempted various reaction conditions ranging from reactions in pure organosilane, to reflux in a two percent solution of the silane in dry solvent, in order to optimize monolayer coverage. Where electron transfer from a bound electrochemically active substance to the electrode surface is desirable, the authors have found the monolayer coverage of the silane at the surface is most desirable.

ESCA (Electron Spectroscopy for Chemical Analysis) analysis showed significant variation in the tin oxide surfaces before and after silanization. Reduction in the intensity of the Sn 3d bands in the 500-480 eV binding energy region, accompanied by the appearance of Si 2p transitions in the 110-100 eV binding energy region were always observed for silane modified SnO_2 surfaces. This type of behavior would be expected for the addition of overlayers of bonded material (see ESCA analysis section).

D. Covalent Attachment to Various Surfaces

Although most electrode surfaces can be modified by adsorption, it would be more desirable to permanently modify a surface by covalent attachment. Methods for securely and

irreversibly anchoring molecules to surfaces could be utilized to produce surfaces with unique and widely varying surface properties.

The binding of proteins to highly porous surfaces was first pioneered by H. Weetall (30). Prior to the development of covalent attachment, proteins were immobilized on chromatographic columns, where they were to be used for sequencing. The experimental basis for sequencing, called Edman degradation, has also been carried out by attaching the protein to a solid support (32). Solid supports used include polystyrene resins, and more recently, derivatized glasses.

Harper (34) accidentally discovered a method of attaching acid-base indicators to porous glass while attempting to activate their surfaces for the binding of proteins. In the process of activation, a pale orange sintered glass funnel was produced, from which the color could not be removed. Washing with acids failed to remove the color, and only turned the funnel reversibly red. These bound-type indicators are claimed to have several advantages over soluble indicators.

The mechanism for attachment is outlined in Figure 3. Initially the surface is modified using a silane, most commonly α-aminopropyltriethoxysilane. The alkylamine glass produced is then coupled to cyanuric chloride by refluxing in a chloroform solution, and to this the indicator, having either an amino, phenolic, or alcohol functional group may be added.

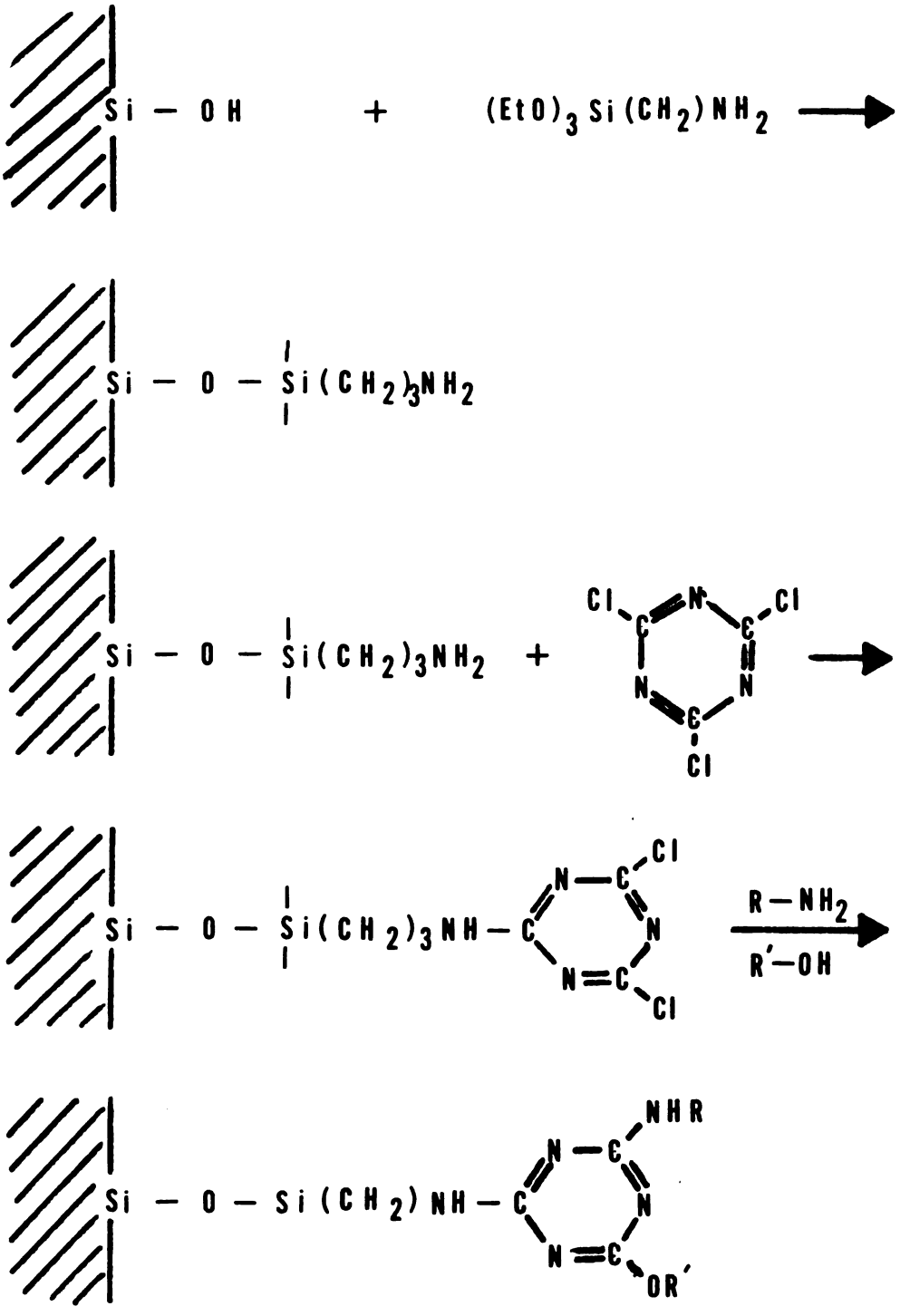

Figure 3. Covalent attachment to surfaces using cyanuric chloride.

Harper used exclusively porous glass, since he noticed little or no retention of the dye on smooth glass surfaces. The fact that these porous glasses irreversibly adsorb dyes indicates that a true covalent linkage may not always be formed.

The bonding of an aniline azo dye to glass slides has been achieved by first treating the surface with thionyl chloride (65). Reaction of the treated surface with an amine group of the dye produced a stable amide bond. The immobilized dye absorption spectral characteristics closely resembled those for the analogous solution forms of the dye. The coverage of the dye, calculated as 1.1×10^{-10} moles/cm^2 (6.6×10^{13} molecules/cm^2) is consistent with monolayer coverage.

The covalent attachment of reversible electrode reactants to various electrode materials have only recently received attention in the literature. Moses and Murray (35) have bound 3,5-dinitrobenzoylchloride, which possesses two electrochemically active nitro groups, to a ruthenium oxide (RuO_2) electrode via 3-(2-aminoethylamino)propyltrimethoxysilane (en-silane). The coupling reaction also involved the formation of an amide, with the loss of HCl. Cyclic voltammagrams of surfaces thus modified showed behavior similar to that for n-butyl-3, 5-dinitrobenzamide in a solution at a RuO_2 electrode. Similar results have also been achieved at platinum electrodes (36). Miller (37,38) has produced a chiral electrode with interesting properties

by bonding an optically active amino acid to a carbon electrode. (S)-(-)phenylalanine methyl ester was attached to electrodes which had first been modified with thionyl chloride, resulting in the formation of an amide bond. For the study of the electrodes, the reduction of 4-acetylpyridine was chosen, in order to verify the success of the attachment. This ketone is reduced at low cathodic potentials to an alcohol. When the reduction is carried out in the presence of the optically active amino acid, an optically active alcohol results. This behavior was observed at chemically modified electrodes. These experiments demonstrated the feasibility of achieving more selective electrochemical processes through electrochemical modification of electrode surfaces.

Murray has also attached aminophenylporphyrins to glassy carbon by a similar attachment procedure (66). Cyclic voltammetric studies of the modified electrodes showed electrochemical behavior consistent with that for the porphyrin in nonaqueous solution. Metallation of the porphyrin ring with cobalt (II) produced cathodic reduction waves consistent with the Co(II) — Co(I) reduction. A similar attempt to bond iron porphyrins using dicyclohexylcarbodiimide to tin oxide electrodes was inconclusive (67). Davis and Murray observed that the porphyrin was irreversibly adsorbed to the surface regardless of whether the surface had been previously silanized or not. Attempts to characterize these electrodes using ESCA spectroscopy were also

inconclusive, since the Fe $2p_{3/2}$ and Sn $3d_{3/2}$ bands occur at almost the same binding energy.

Fujihira, Matsui, and Osa (39) have studied the double-layer capacitance of ESCA behavior of tin oxide electrode surfaces modified with p-nitrobenzoylchloride via an organosilane. ESCA spectra of the modified surfaces showed a nitrogen 1S band consistent with the presence of a nitro group at the surface. Cyclic voltammagrams verified a cathodic redox process consistent with the known electrochemistry of the nitro group.

Double-layer capacitance measurements indicated little difference in the slope of the Mott-Schottkey plots, indicating little difference in the carrier density of the tin oxide surface for the bonded or unbonded case. A significant increase in the flatband potential toward more cathodic values was observed. This change was attributed to an increase in the potential drop across across the Helmholtz layer, which would be expected upon the addition of a low-conductivity organic group to the electrode surface. Recently Fujihira (4) reported the covalent attachment of Rhodamine B dye to a tin oxide electrode. The photocurrent action spectrum of the dye-modified electrode mimicked the ultraviolet-visible spectrum of the dye. Cyclic voltammetric behavior or ESCA data were not reported for these electrodes.

E. Dye Materials

Fluorescein and erythrosin have been used for color copied images in photography (74). Transfer plates for the

copied images were made of a dispersion consisting of ZnO_2, butadiene-vinyltoluene polymer, fluorescein, methylene blue, and Rose Bengal. Harper (45) has produced insoluble indicators covalently bound to glass surfaces. The dye and carrier were bound via a silane coupling agent, using a sulfonamide linkage. These dyes have also been investigated for possible use as laser sources, using THF, ethanol, or water as solvents (41). Ionov and Akimov (42) have used erythrosin for the spectral sensitization of the photoelectric effect in narrow-band semiconductors. Measurement of the photoconduction of germanium, silicon, lead sulfide, and selenium crystals coated with a thin film of the dye showed a spectral sensitizing effect due to the dye, with a very high efficiency.

F. Historical Conclusion

The study of tin oxide surfaces and their modification has been presented. Although there has been much recent research on these semiconductor surfaces and their silane modification, the field of covalent attachment of dye molecules is relatively new and unstudied. It is the goal of this research to thoroughly study, by both electrochemical and surface analysis means, dye modified surfaces. In this way we may be able to learn more about the properties of modified surfaces.

The photocurrent sensitizing effect of these and other dyes either adsorbed, or more recently, covalently attached to electrode surfaces, is also a well-studied phenomenon.

Little is known about the photoefficiency of such surfaces, however. Further, we do not know how critical a covalent linkage is to photocurrent production. The entire goal of this research will be to answer these questions.

CHAPTER II

ESCA ANALYSIS

Among the many new instrumental techniques developed in recent years, electron spectroscopy for chemical analysis (ESCA) is one of the most ideally suited for examination of surfaces. It is sensitive to almost every element, and its signal can be used as either a qualitative or quantitative tool.

The ESCA technique was developed by Kai Siegbahn at Uppsala University in Sweden. His early work is well documented in two books (68,69), which outline in detail the principles involved.

The ESCA instrument is composed of five basic parts: (1) a source, (2) high vacuum sample chamber, (3) electron energy analyzer, (4) detector, and (5) readout systems.

Bombardment of the sample by high energy x-ray photons causes the emission of electrons from the core and valence bands of the bombarded sample. For ESCA analysis, these core electrons are most important, because the energies with which they leave the parent atom are well defined and specific to the parent atom. The electrons emitted from the sample, commonly called photoelectrons, leave the parent atom with kinetic energies which are a function of the incident photon energy, the energy required to cause their removal from the parent atom, and the work function of the spectrophotometer. While the energy required to remove the electron from its parent atom varies from atom to atom, all other parameters remain constant. Therefore, the kinetic energy which the electron has when it reaches the analyzer is unique to a

particular atomic species. Further, these photoelectrons, because of their relatively low kinetic energies, can escape from only the top few monolayers of material. Normally, the kinetic energies the photons have upon reaching the analyzer are converted to binding energies, ranging from 0 to 1000 electron volts. ESCA analysis can be used to qualitate atomic species present at a surface. Since the binding energies are very specific to the environment of the atoms in the sample, binding energies can also be used to determine the oxidation state for various atoms at the surface.

Use of ESCA analysis to determine overlayer thickness on a substrate is one of the more valuable pieces of information this technique can supply. Bonding or adsorption of overlayers of material on a surface causes a reduction of the ejected photoelectron intensities from the underlying sample. This decrease in intensity for a particular component can be used to determine overlayer coverage. In this type of quantitation work, however, it is necessary to know the mean free path, or escape depth of electrons from the underlying sample. These values vary from element to element, and also depend to a small extent on the material composing the overlayer. These values have been tabulated for several elements (71).

The appropriate equation for calculation of overlayer thickness is

$$I/I_{clean} = \exp(-d/\lambda)$$

Both I and I_{clean} represent the intensities of the native

photoelectron before and after overlayer coverage, respectively. λ is the escape depth for the photoelectron through the material, and d is the overlayer thickness. For the tin $3d_{5/2}$ photoelectrons, λ is normally taken as 11 Angstroms (71). Murray and coworker (64) have used this method with moderate success to calculate overlayer coverages of silane bonded to tin oxide.

Although values for the amount of material present at a surface cannot be absolutely determined, these can be calculated relative to some element present and measureable at the surface. For example, Armstrong and coworkers (72,75) have determined relative amounts of oxide on tin oxide or titanium oxide surfaces, by ratioing the oxygen to titanium or oxygen to tin intensities. This method can then be used to determine surface stoichiometry for a particular material.

Since the excitation source for ESCA, x-ray radiation, does not affect all atoms the same, corrections must be made for this occurrence. For a given number of photons striking the surface, different numbers of photoelectrons are produced for each element. Therefore, intensity ratios must be corrected by multiplying the values by their relative photoionization cross sections. Values for most common elements have been tabulated by Scofield (55).

CHAPTER III

EXPERIMENTAL SECTION

A. Electrochemistry

All electrochemical measurements were performed on a four or five-amplifier potentiostat of conventional design (73). The circuit diagrams for both configurations are shown in Figures 4 and 5. Each has external connections for auxillary, reference and working electrodes, with the working amplifier acting as either a voltage follower (Figure 4) or as a current-to-voltage converter (Figure 5). In the second case, various precision resistors could be substituted into the feedback loop of the operational amplifier for different current sensitivities, ranging from 10uA/mv to 1 uA/mv out. For low-frequency chopped photocurrent measurements, the operational amplifier could be capacitively damped to limit noise contributions.

Double-throw switch S_1 could be used to apply external bias, as regulated by variable resistor R_1. External inputs W_1 and W_2 could be used to apply various external waveforms. A compensation circuit was also connected through single-throw switch S_2 for compensating for IR drop between working and auxillary electrodes.

Double-layer capacitance measurements were made according to the method of Gileadi (13). This method involves application of a sine wave signal superimposed on an applied bias potential. In this manner, electrode capacitance can be investigated at various externally applied potentials. A small amplitude sine wave was used (less than 20 mV peak to peak) in a 300-800 Hz frequency range, in order to limit faradaic contributions.

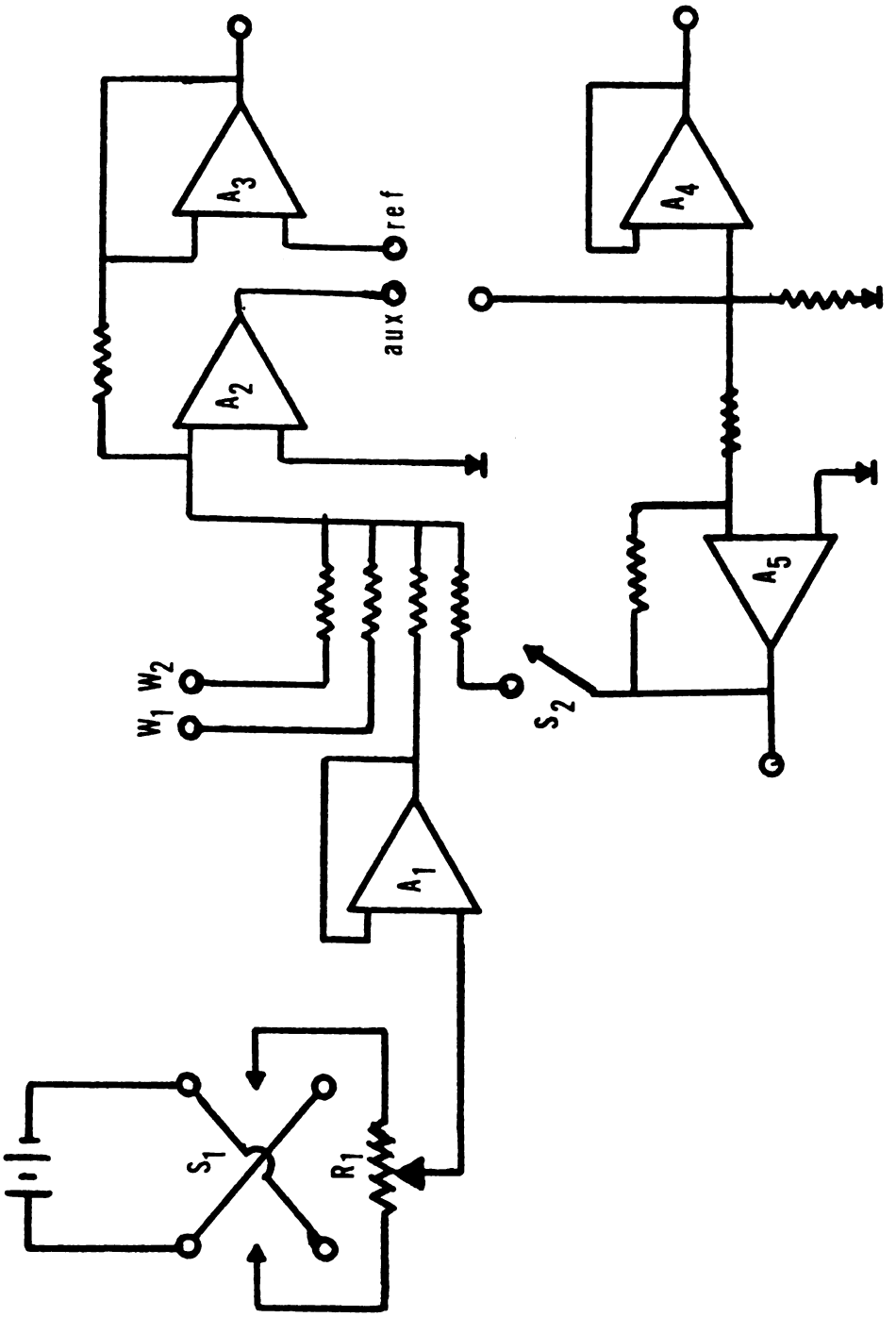

Figure 4. 5-operational amplifier potentiostat.

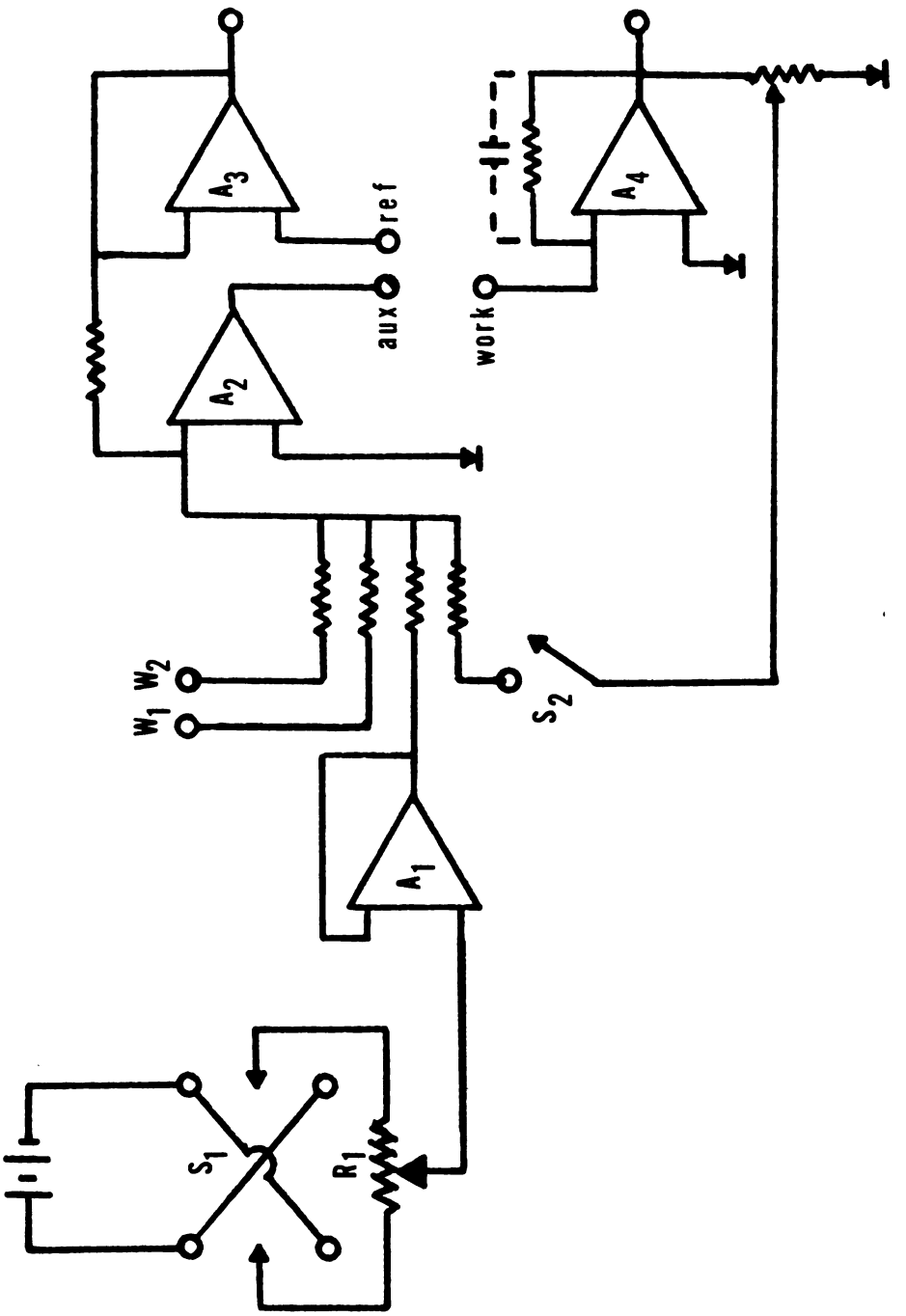

Figure 5. 4-operational amplifier potentiostat.

As long as the impedance measured at the electrode is mainly capacitive, the response to a small triangular wave is a square wave whose amplitude is proportional to the capacitance. Any IR drop through the solution is easily compensated for. The working amplifier is acting as a differentiator, with the electrode capacitance acting as a capacitor in a circuit. After correct compensation had been achieved, using a triangle wave, a sine wave was substituted. Capacitance measurements were performed in pH 7 phosphate buffer of approximately 0.1 ionic strength. Current output was measured by using a phase-sensitive lock-in amplifier (Princeton Applied Research, Model 126).

Cyclic voltammetric studies were performed with the same potentiostat, using an externally applied ramp function of varying slope and range. Current-voltage output was recorded with a Houston Series 1100 X-Y recorder. For electrochemical adsorption of various dyes at the electrode, the charge passed was measured using a digital coulommeter built in this department. Chronoamperometric data were recorded on a Heath strip chart recorder. For all measurements, the potential was stepped to +1.0 volts measured against a $Ag^{+}/AgCl$ reference.

B. Photoelectrochemical Measurements

The light source used for photocurrent generation consisted of an Electropowerpacs power supply and Oriel universal lamp housing, with a 450 or 1000 watt Hanovia Zenon arc lamp.

The lamp output was passed through a 6-inch water filter to remove infrared wavelengths, followed by an infrared interference filter. A set of Oriel interference filters was used to isolate the wavelength desired. A variable frequency chopper was used at 13 Hertz for these measurements. The potentiostated photocurrent was measured using the lock-in amplifier previously mentioned, which was triggered by the chopper output.

Photocurrent measurements were performed at a bias of +1.0 volts against a silver/silver chloride reference. The electrolyte used was pH 4 buffer which had been made 0.1 M in pottasium oxalate.

C. Electrochemical Cells

The new principle types of cells used are shown in Figures 6 and 7. The cell of circular design was constructed of lucite, with two glass stopcocks for filling and emptying. The reference electrode consisted of a glass tube with a ¼-inch thirsty quartz frit (Corning Glass Works, Corning, New York) sealed at one end with heat-shrinkable tubing. A silver wire deposited with silver chloride, dipping into a saturated potassium chloride solution, acted as an $Ag^+/AgCl$ reference. A short length of platinum wire, coiled and sealed in the cell, served as auxillary electrode. The working electrode was sealed in the end of the cell by a Viton O-ring, and held by a lucite face plate and screws. Exposed electrode area, calculated from chronoamperometric

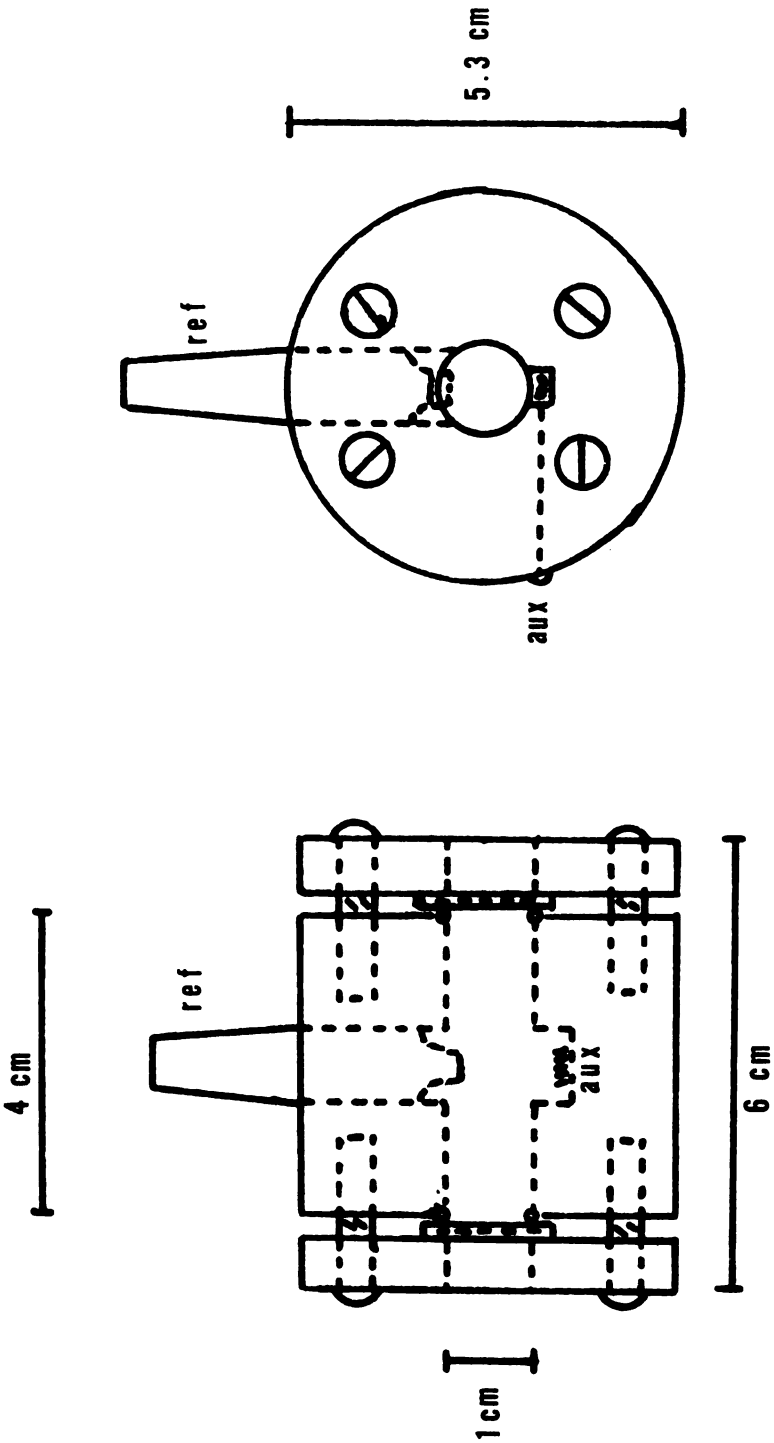

Figure 6. Circular electrochemical cell constructed of Lucite.

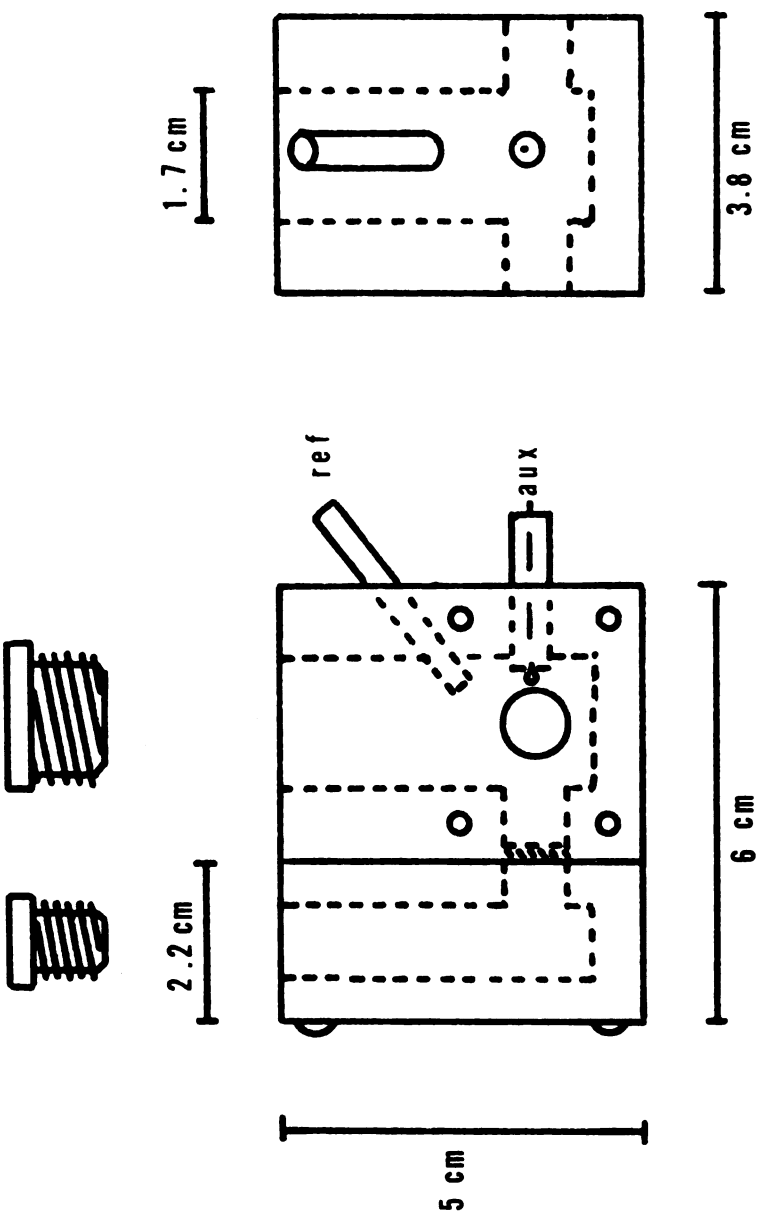

Figure 7. Electrochemical cell constructed of Teflon or Lucite.

data, was 0.636 cm^2. Electrical contact was made by a circular brass contact pressed against the electrode surface concentric with the exposed electrode area. This insured that, for tin oxide layers on nonconducting bases, the series resistance was as low as possible to facilitate capacitance measurements at higher frequencies. Such a contact configuration also minimized capacitance dispersion due to distributed resistance of the thin film.

The rectangular cell shown was constructed of either lucite or teflon. The teflon cell was used where aqueous dye solutions were investigated. In this way, the cell could be disassesmbled and cleaned in a suitable solvent. The auxillary electrode compartment was separated from the working electrode compartment by a fine glass frit. With this configuration, any products produced at the auxillary electrode could be kept from contaminating the working electrode.

D. Materials and Reagents

Vapor-deposited tin oxide on glass was obtained from Pittsburgh Plate Glass (Pittsburgh, Pennsylvania). The films, of approximately 4-7000 Å thickness, were either fluoride or antimony doped. The plates were cut into squares approximately 2 cm on a side prior to use.

Toluene (Drake) was dried in magnesium sulfate and distilled from potassium metal prior to use. Tetrahydrofuran (Mallinkrodt) was dried by the same procedure. Both were distilled under nitrogen atmosphere.

3-(2-aminoethylamino)propyltriethoxysilane, mercaptopropyltrimethoxysilane (Dow Corning), and α-aminopropyltrimethoxysilane (ICN) were not purified prior to use. All silanes were stored in a freezer when not in use. Dyes (Eastman Kodak) were used as is. Erythrosin was dried in a vacuum oven at 35-40° C for twenty-four hours prior to use in the amide reaction.

Dicyclohexylcarbodiimide (DCC) (ICN) was used as obtained from the manufacturer.

E. Aqueous Solutions

All solutions were prepared in doubly-distilled deionized water and deoxygenated by bubbling thoroughly with nitrogen gas.

Either pH4 or pH 7 buffers were prepared using potassium hydrogenpthalate (KHP) and nitric acid, or potassium dihydrogen phosphate and sodium hydroxide. 1.0 millimolar ferrocyanide solutions were prepared in pH 4 buffer using potassium ferrocylencide ($K_4Fe(CN)\cdot 6H_2O$).

F. Covalent Attachment of Dyes

The SnO_2 surfaces were prepared for silanization by first washing the electrodes in a detergent solution, followed by washings in ethanol and distilled water, using an ultrasonic cleaner. The surface was activated prior to reaction by refluxing in 0.1 N HNO_3 for two hours. This step assured that all tin oxide surface sites were protonated, allowing more complete silane coverage. Finally, the electrodes were

rinsed in ethanol, followed by drying in vacuum.

The conditions for silanization are shown in Table 1. Special care was taken to exclude air during the reactions as much as possible. In this way, cross-polymerization of the silane groups could be held to a minimum.

Table 1. Conditions for Silanization

Silane	Solution	Reaction Conditions
-aminopropyltrimeth-oxysilane	5% in dry Toluene	12 hours reflux
3-(2-aminoethylamino)-propyltriethoxysilane	1% in dry Toluene	½ hour reflux
mercaptopropyltrimeth-oxysilane	2-5% in dry	1 hour, no reflux

After silanization, the electrodes were washed in portions of the dry toluene solvent, and refluxed for one to two hours to remove excess unbonded reagent. The degree of surface coverage was extremely difficult to control, and varied between batches of tin oxide.

1. Thiol Attachment. Tin oxide electrodes which had been modified with the mercaptosilane ($SH\text{-}SnO_2$) were placed in a pH 7 buffer solution (0.1 ionic strength) which was 1.0×10^{-3} M in erythrosin dye. The reaction was allowed to proceed twelve hours at room temperature, with continuous stirring, under nitrogen atmosphere. Excess dye was removed from the surface by extended period of extraction in a sohxlet apparatus using either ethanol, acetone or water as solvent.

2. Amide Attachment. For the amidization reaction, several solvents were investigated, the most satisfactory of which was tetrahydrofuran. Carbon tetrachloride and nitrobenzene are other widely used solvents for amidization reactions, but neither worked successfully for the attachment reaction. The relative reaction rates for these three solvents are 34:18:1 (CCl_4: Nitrobenzene: THF) (61).

A 1.0 mM solution of erythrosin dye, previously dried, was prepared in dry THF. The THF/dye solution was cooled to 0^{o} C in an ice bath, after which a stoichiometric amount of DCC, which was dissolved 10% w/w in THF, was added dropwise. The solution was allowed to stand fifteen minutes, then the amine-modified electrodes were added. The reaction was allowed to proceed in the dark, with continuous stirring, for forty-eight hours. The modified electrodes were extracted afterwards to remove excess dye. The covalently modified electrodes could be stored for extended periods of time in the dark, but showed almost complete bleaching of the dye after two weeks in light conditions.

G. ESCA Data

ESCA (Electron Spectroscopy for Chemical Analysis) spectra were obtained on a Physical Electronics Model 548 instrument, using a magnesium anode source operating at 400 watts. Vacuum was maintained at 10^{-8} torr or lower. For signal averaging, the instrument was interfaced to a Data General Nova-800 computer with 32k core memory. For overall spectra, pass energy was set at 100eV, using a scan rate of

7 eV sec^{-1}. High resolution spectra of the tin $3d_{5/2}$ and $3d_{3/2}$ bands were obtained using a 20 eV window, from 500 to 480 eV, with a pass energy of 25 eV. In the case of the iodine $3d_{5/2}$ and $3d_{3/2}$ bands, a 50 eV window (650-600 eV) with 50 eV pass energy was used. These pass energies were selected to optimize the signal-to-noise ratio.

H. Deconvolution

ESCA spectra were deconvoluted into their individual components by methods similar to those previously published (72). The spectra were deconvoluted by computer simulation of the total spectrum using the suspected components present. The simulation program used the following parameters: (1) the slope of a linear background, (2) the binding energy of each component, (3) the full width at half maximum of each component (FWHM), (4) the peak heights of each component, and (5) the percent Gaussian and Laurentian contributions to the total line shape. Parameter 3 was evaluated from standards made of pressed pellets of erythrosin in sodium chloride or SnO_2 powders. Parameter 5 was typically 50% for the pass energies used. All reported binding energies were corrected for charging effects by referencing to the Sn $3d_{5/2}$ band at 486.2 eV (12). Simulations were performed on a PDP-11 computer coupled to a Vector General CRT display. Hard copies of spectra could be obtained after simulation on a Versatek plotter.

A. Introduction

The structures of rhodamine B, erythrosin and fluorescein are shown in Figure 8. Note that fluorescein dye is simply the unhalogenated form of erythrosin. At pH = 7, rhodamine B is a cation, since the phenolic group has a pK of 9 (7). Similar behavior would be expected for both fluorescein and erythrosin at this pH.

Varying the pH only slightly affects the wavelength of maximum absorbance in erythrosin, indicating that the carboxylic acid group has little to do with the light-absorbing process. Comparing the wavelengths of maximum absorbance for erythrosin and fluorescein, however, indicates that the substitution of iodine groups on the conjugated ring system of the dye strongly affects the absorption process. As Figure 9 shows, erythrosin at pH = 7 has a λ_{max} at 536 nm, whereas fluorescein has a maximum absorbance at 489 nm.

This indicates that, for erythrosin, the ground state of the dye is separated from the lowest excited state by 2.32 electron volts. This separation is 0.22 eV less than fluorescein, where 2.54 eV separates the ground and lowest excited states. This trend is consistent with expected behavior, since the addition of an electron-donating group such as iodine should make it easier to excite electrons in the ring structure from ground to the lowest excited state.

The principle motivation for using a halogenated dye was to allow quantitation of the modified surfaces using ESCA analysis. Although all the dyes previously mentioned

A. Introduction

The structures of rhodamine B, erythrosin and fluorescein are shown in Figure 8. Note that fluorescein dye is simply the unhalogenated form of erythrosin. At pH = 7, rhodamine B is a cation, since the phenolic group has a pK of 9 (7). Similar behavior would be expected for both fluorescein and erythrosin at this pH.

Varying the pH only slightly affects the wavelength of maximum absorbance in erythrosin, indicating that the carboxylic acid group has little to do with the light-absorbing process. Comparing the wavelengths of maximum absorbance for erythrosin and fluorescein, however, indicates that the substitution of iodine groups on the conjugated ring system of the dye strongly affects the absorption process. As Figure 9 shows, erythrosin at pH = 7 has a λ_{max} at 536 nm, whereas fluorescein has a maximum absorbance at 489 nm.

This indicates that, for erythrosin, the ground state of the dye is separated from the lowest excited state by 2.32 electron volts. This separation is 0.22 eV less than fluorescein, where 2.54 eV separates the ground and lowest excited states. This trend is consistent with expected behavior, since the addition of an electron-donating group such as iodine should make it easier to excite electrons in the ring structure from ground to the lowest excited state.

The principle motivation for using a halogenated dye was to allow quantitation of the modified surfaces using ESCA analysis. Although all the dyes previously mentioned

a.

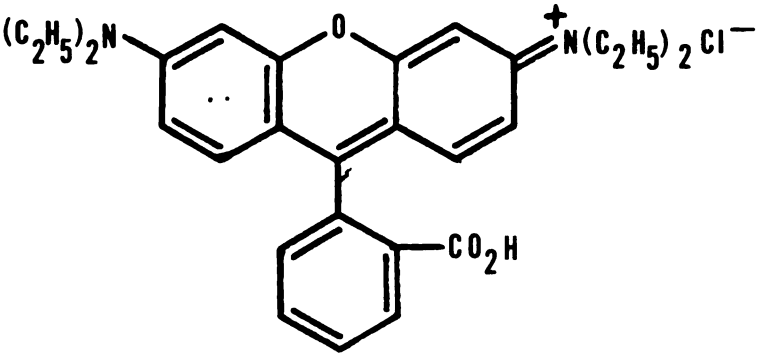

b.

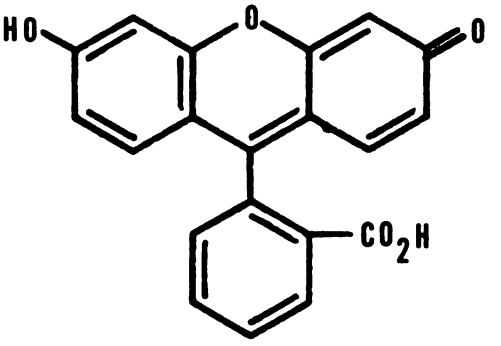

c.

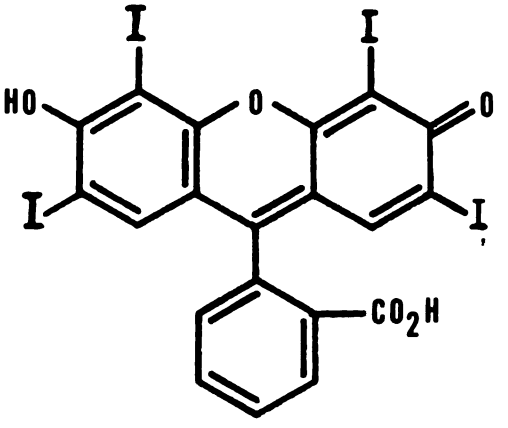

Figure 8. Structures of various dye molecules; a. Rhodamine B, b. Fluorescein, c. Erythrosin.

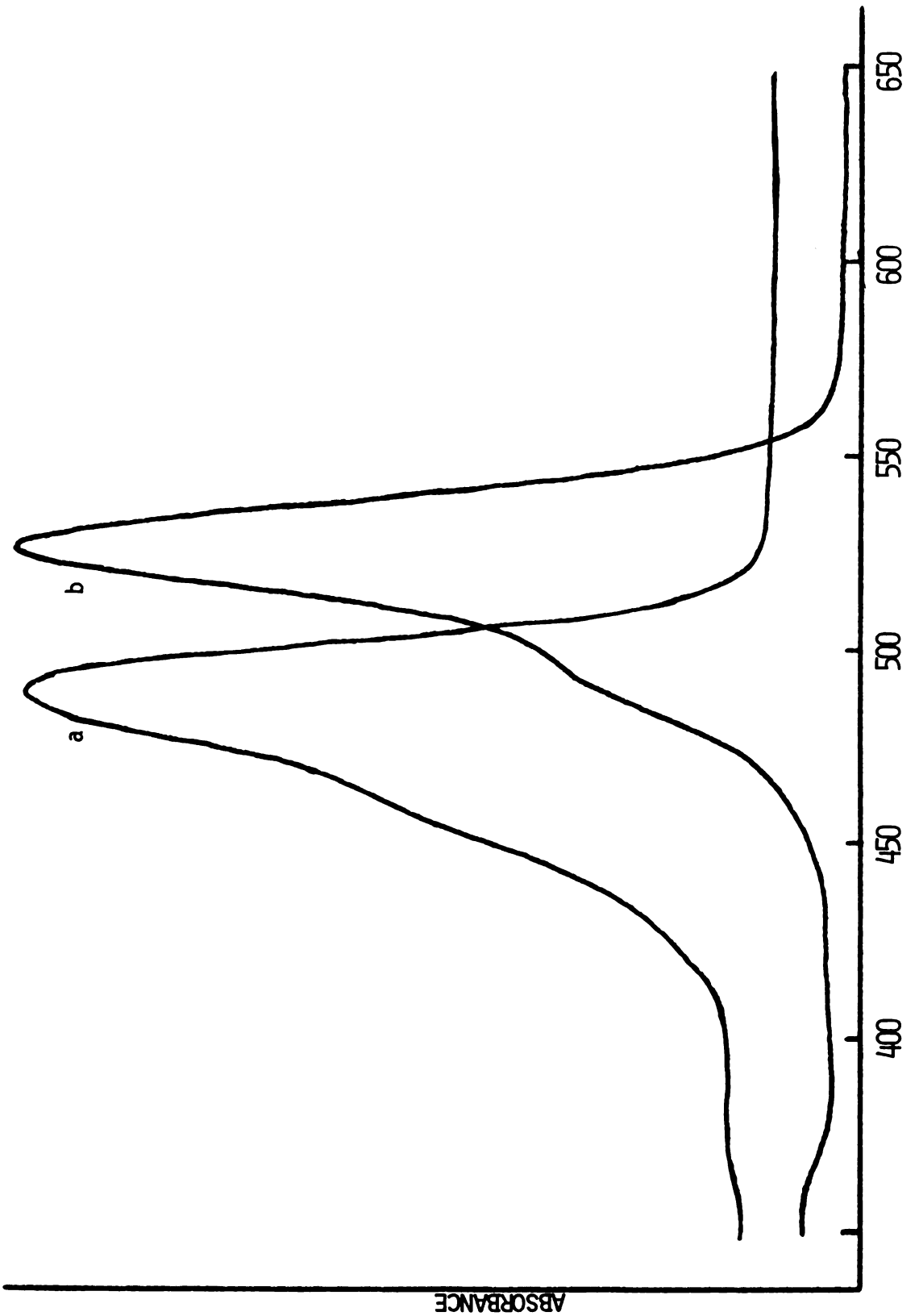

Figure 9. UV-visible spectrum of dyes in pH 7 buffer; a. Fluorescein, b. Erythrosin.

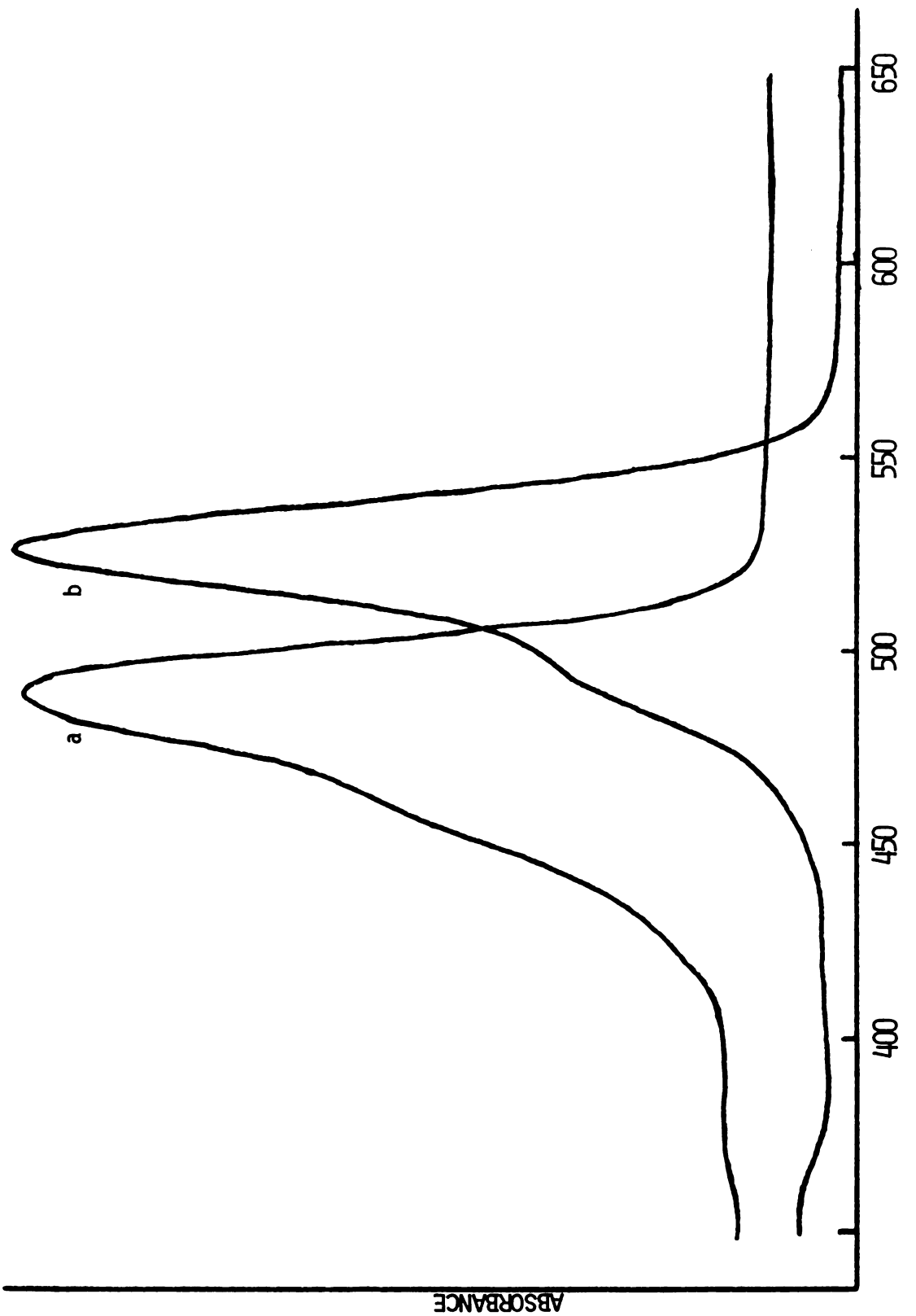

Figure 9. UV-visible spectrum of dyes in pH 7 buffer; a. Fluorescein, b. Erythrosin.

contain carbon, nitrogen and oxygenations, these are not satisfactory for ESCA analysis, since they can also be present at the surface as contaminants resulting from air or solution exposure. Therefore, by providing an unambiguous tag atom, with a favorably high molecular cross section, surface analysis could be employed.

B. Electrochemical and ESCA Analysis of Multilayer Dye Assemblies

The electrochemical behavior of erythrosin is interesting and has led to a rather unique way of constructing multilayer dye assemblies at the electrode surface. The cycle voltammetric behavior of the dye on a clean tin oxide electrode surface is shown in Figure 10. The concentrations of dye in pH = 7 buffer range from 5.0×10^{-4} M (Figure 10a) to 5.0×10^{-5} M (Figure 10d). The cyclic shows that the dye has a peak potential on clean tin oxide of .875 volts, as measured against a silver/silver chloride reference. Figure 10e shows a 5.0×10^{-4} M dye solution, also on a clean electrode surface. The observed cathodic shift in the case is due to the quality of the tin oxide, its doping level, and film thickness. It is not uncommon to notice a variation between batches of tin oxide made by the same manufacturer. In order to make the results presented in this section more reliable, we were careful to use the same quality of electrode material throughout a particular experiment, or where comparisons were to be made between separate experiments.

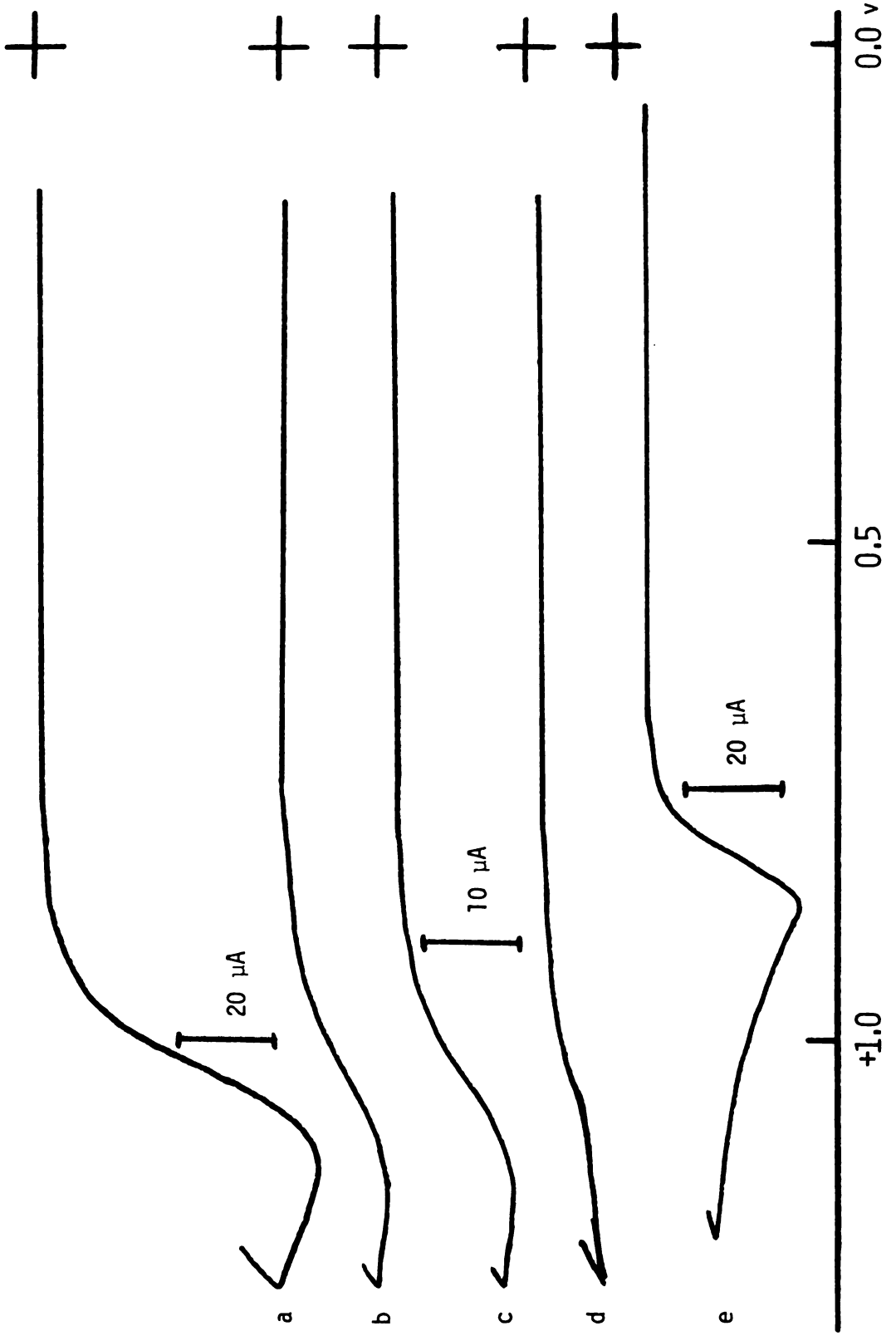

Figure 10. Cyclic voltammetric behavior of Erythrosin dye on clean SnO_2 at various concentrations; a = 5.0×10^{-4} M, b = 2.5×10^{-4} M, c = 1.0×10^{-4} M, d = 5.0×10^{-5} M, e = 5.0×10^{-4} M.

The charge passed in each cyclic voltammagram increases with increased dye concentration, as is apparent in the Figure. There is little effect on the peak potential with varying concentration, although at lower concentrations much of the observed background slope is due to the proximity of the anodic limit of SnO_2 to the peak potential.

This electrochemical phenomenon can be attributed to a simple adsorption process at the electrode (48), similar to the behavior of chloride at SnO_2 surfaces (4). There is no precedent to indicate that the dye is undergoing an oxidation process, although this may also be occurring. A chemisorbed phase at the electrode surface may be formed by this faradaic process. The observed behavior might be due to charging and discharging of position surface states (tin atoms), caused by a dipole-dipole or dipole-ion interaction with the dye (56,63). This configuration would be more or less equivalent to the charging of a capacitor. The reverse scan does not produce a reduction wave anywhere in the full potential region of SnO_2.

Comparing the peak potentials of erythrosin and rhodamine B at clean tin oxide, there is a cathodic shift of 190 millivolts for erythrosin, as shown in Figure 11.

Rinsing the unmodified tin oxide electrodes with either water or ethanol after electrochemical adsorption of the dye quickly removed any remaining visible traces, although ESCA data indicated that a tightly bound form of the dye was still present at the electrode surface of about 10 to 20 monolayers.

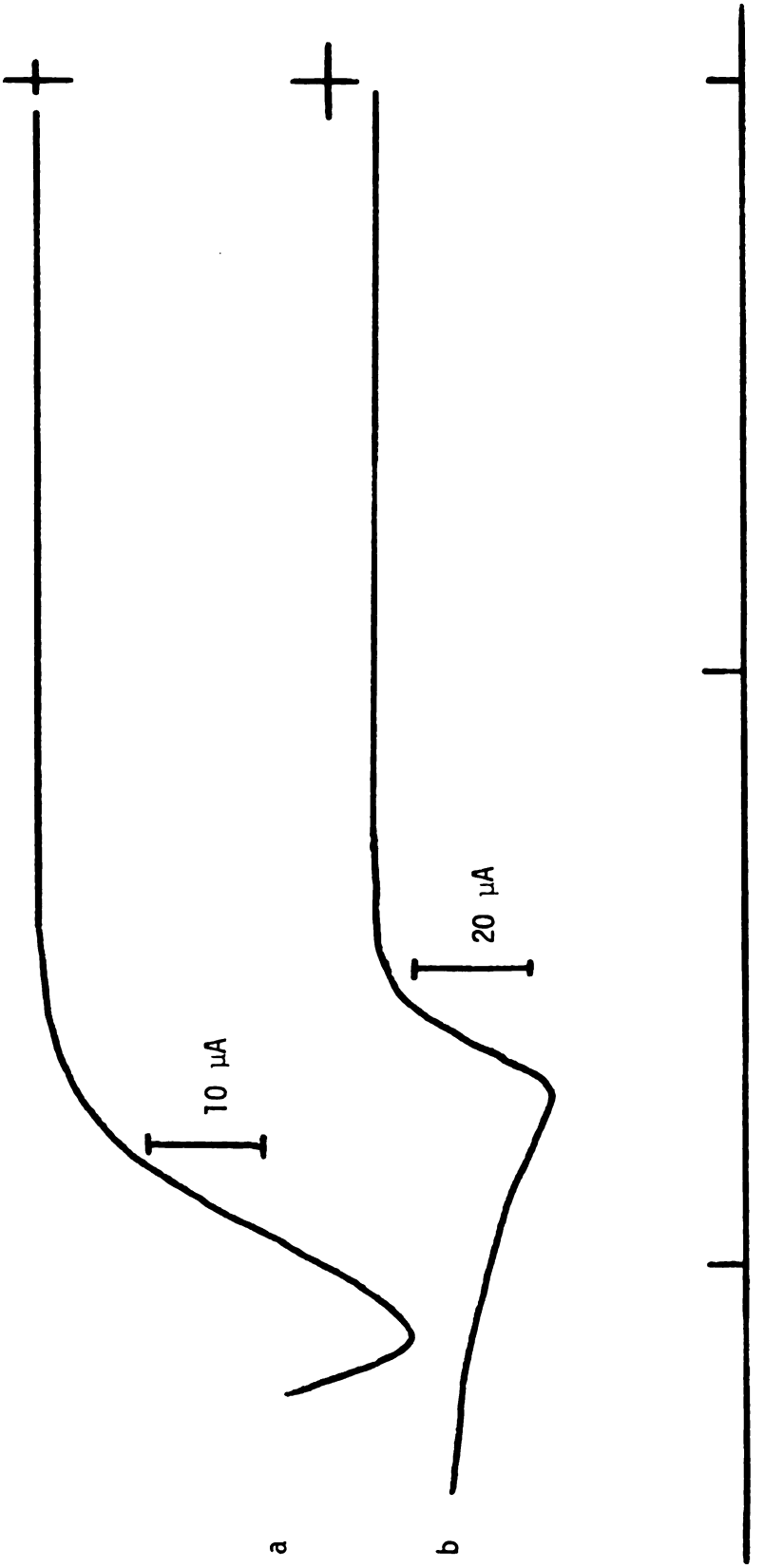

Figure 11. Cyclic voltammetry of dyes at 2.5×10^{-4} M in pH 7 buffer; a. Rhodamine B, b. Erythrosin.

Silanization of the tin oxide surfaces with either α-aminopropyltrimethoxysilane(pr-silane) or 3-(2-aminoethyl-amino)-propyltriethoxysilane(en-silane) caused the peak potential for the erythrosin adsorption to shift approximately 50 millivolts cathodic relative to clean tin oxide. However, examination of the shape of the anodic wave indicated that there was a considerable broadening of the wave for the silane-modified case. Further, the amount of charge passed was about 30% greater for the silane modified case. This indicates that the presence of the terminal amino group at the tin oxide surface had some catalytic effect on the adsorption or oxidation process.

Varying the solution dye concentration for the pr-silane modified electrodes also produced some interesting information in the cyclic voltammetry, as can be seen in Figure 12. As the dye concentration increased from 5.0×10^{-5} M to 5.0×10^{-4} M, there was an apparent cathodic shift of the peak potential toward more cathodic values. Further examination of these voltammagrams, however, indicated that the anodic process appeared to be made up of two anodic waves, which varied in their relative magnitude with varying concentration. At lower concentration, the more anodic of the two processes dominated, whereas at an intermediate (2.5×10^{-4} M) dye concentration, the magnitude of both faradaic waves appeared to be equal. Comparing the shapes of the anodic waves for clean and pr-silane modified electrodes tended to confirm this.

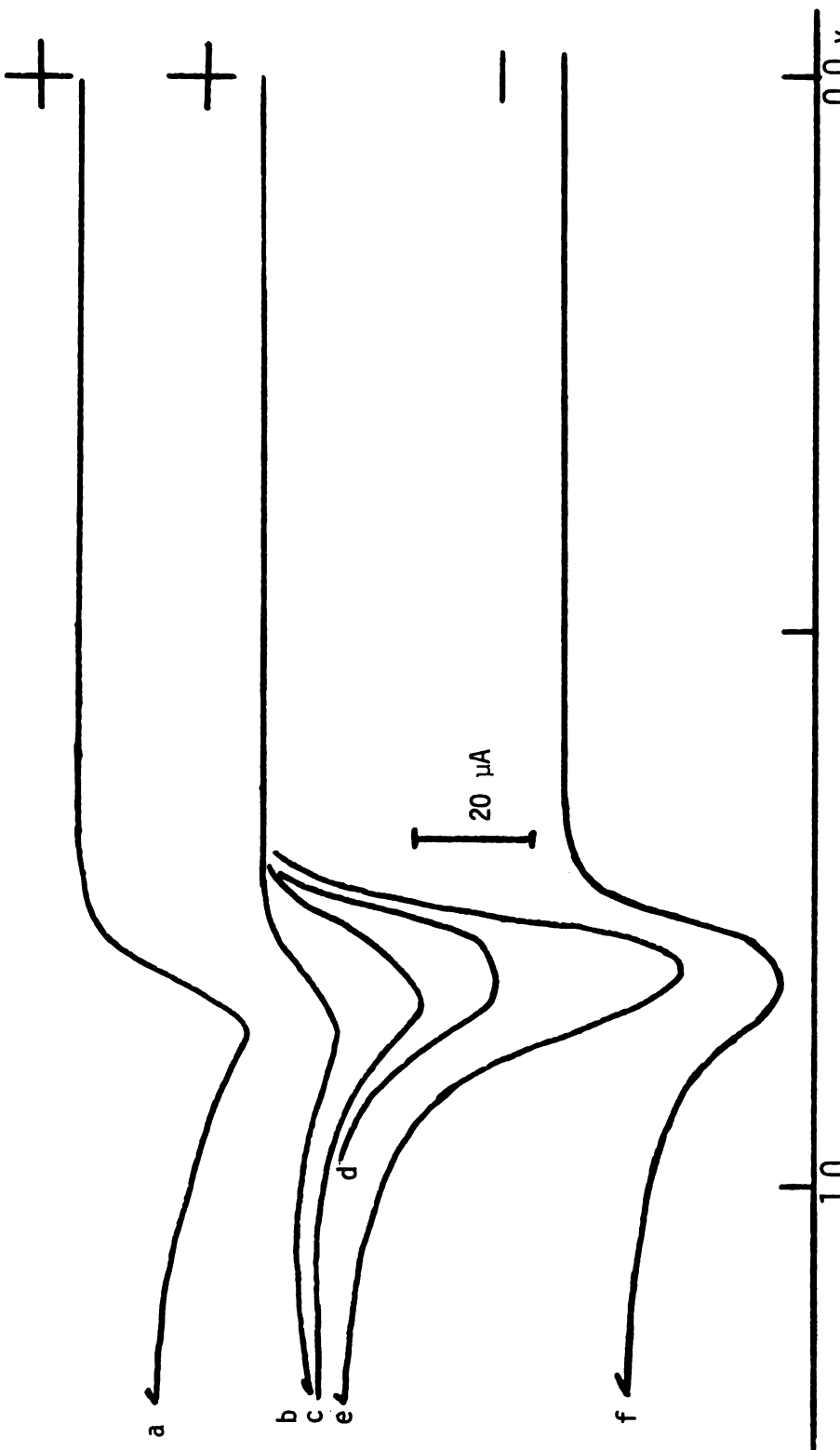

Figure 12. Cyclic voltammetry of dye at pr-silane and en-silane modified electrodes at various concentrations. a. clean SnO_2, 2.5 x 10-4 M; b. 5.0 x 10-5 M; c. 1.0 x 10-4 M; d. 2.5 x 10-4 M; e. 5.0 x 10-4 M; f. 2.5 x 10-4 M on en-silane modified SnO_2.

Unlike clean (unmodified) tin oxide electrodes, rinsing the pr-silane electrodes after dye adsorption failed to remove all visible traces of the dye, so that the electrodes showed a distinct red area where the dye had been adsorbed. Extended periods of soaking in either ethanol or water also failed to remove this tightly held layer from the surface.

Figure 12f also shows a cyclic voltammagram of the dye, at 2.5×10^{-4} M, at a tin oxide electrode modified with the en-silane. The peak potential, the amount of charge passed, and the peak shape appear to be identical to that for the pr-silane modified electrodes at the same concentration (Figure 12d).

A series of electrodes which had been modified with pr-silane, en-silane, and a clean electrode were carried through the electrochemical adsorption, washed in ethanol and water, and transferred to the sample chamber for ESCA analysis at 10^{-9} torr or lower. The resulting iodine high resolution spectra, in the 650-600 eV binding energy region, are shown in Figures 13 and 14, along with their computer-deconvoluted components. The binding energy for the iodine $3d_{5/2}$ bands were corrected for charge shift by referencing to the Sn $3d_{5/2}$ band at 486.2 eV (12).

Figure 13a shows the high resolution iodine bands for the dye electrochemically adsorbed, at 2.5×10^{-4} M, on a clean tin oxide electrode. The larger peak at 621 eV binding energy (I $3d_{5/2}$) as well as the accompanying band at 632 eV (I $3d_{3/2}$) are due to the iodine covalently attached to the

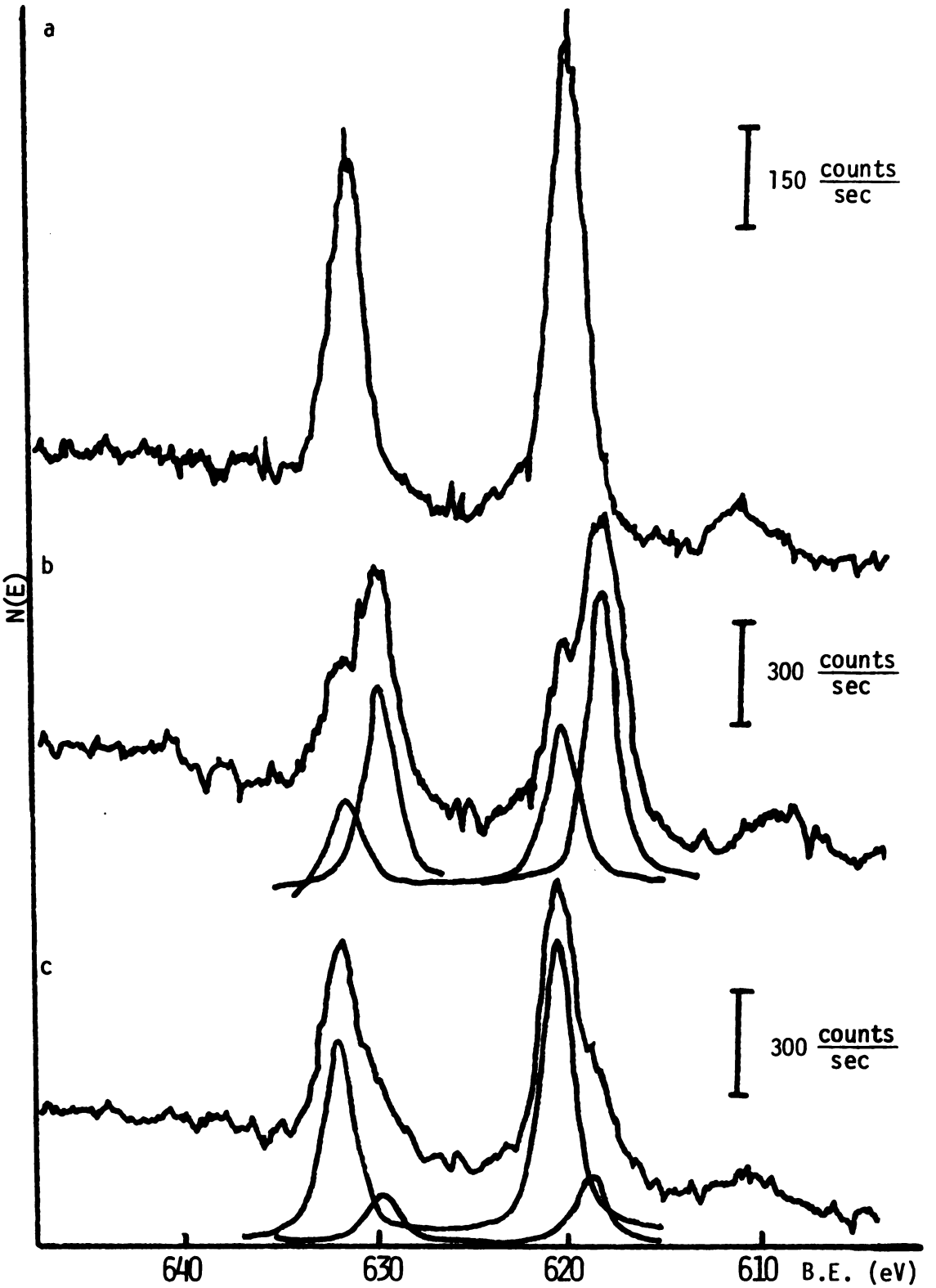

Figure 13. ESCA spectrum of adsorbed dyes on tin oxide surfaces.

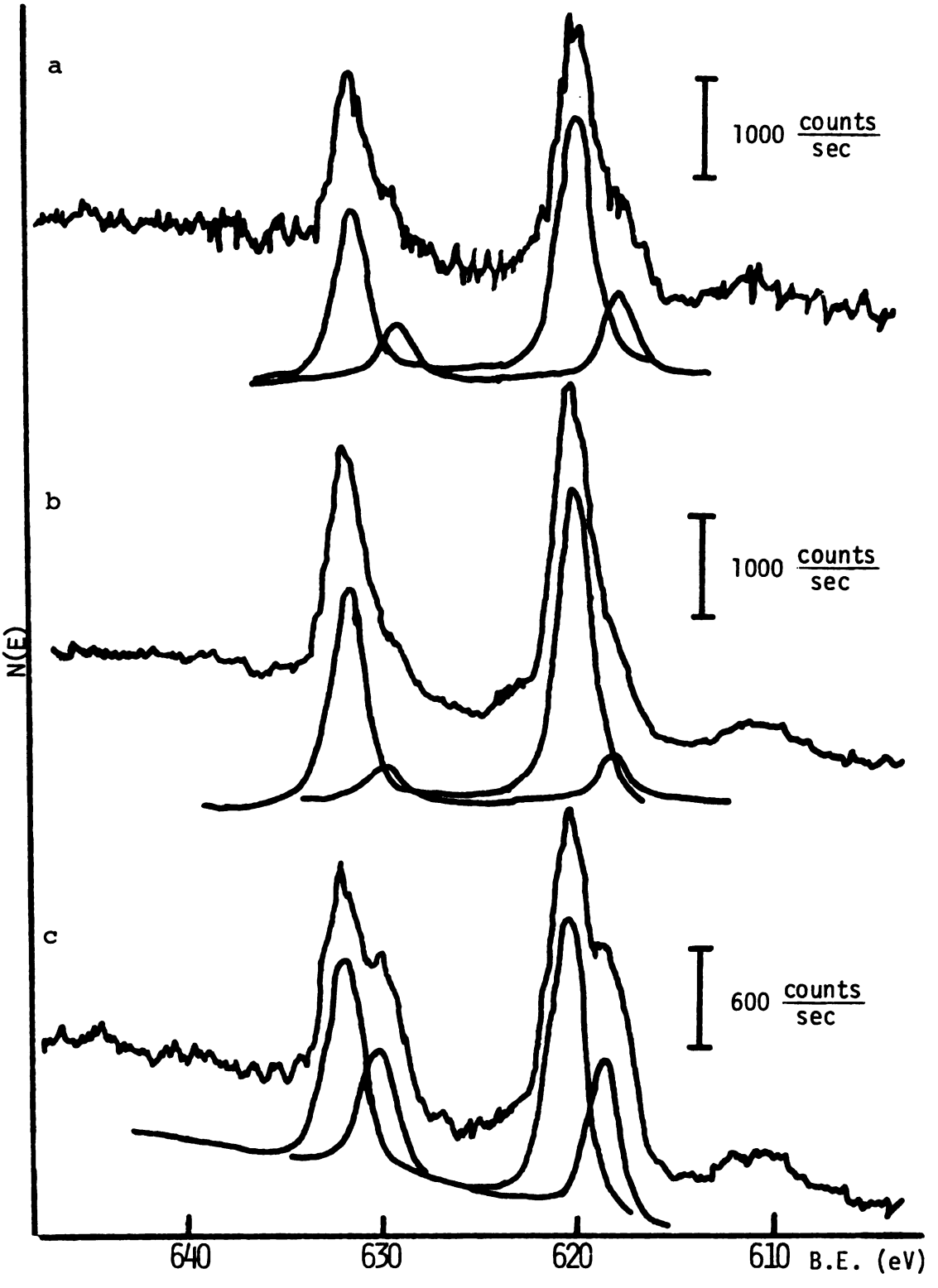

Figure 14. ESCA spectrum of adsorbed dyes on tin oxide surfaces.

dye rings. This was verified by running the spectrum of an electrode to which the dye had been mechanically adsorbed.

After silanization of the surface with pr-silane, and subsequent electrochemical dye adsorption, both I 3d bands showed splits into doublets, the magnitude of which depended on the concentration at which the dye was adsorbed. At the lowest dye concentration (5.0×10^{-5} M), as shown in Figure 13b, the predominant peak for the iodine transition is located at 618 eV binding energy, with a second band at 621 eV. Varying the dye concentration in solution, which subsequently increased the total charge passed, resulted in an increased intensity for the higher binding energy 621 eV band, while the lower binding energy peak was greatly diminished. At the highest concentration used (5.0×10^{-4} M), as shown in Figure 14b, the lower binding energy band is only a minor component in the spectrum, so that its relative magnitude can only be approximated.

Spectra shown in Figures 14a and 14c also merit further consideration. These show high resolution spectra for the pr-silane and en-silane modified tin oxide electrodes, respectively. Both surfaces have undergone electrochemical adsorption of the dye at the same concentration (2.5×10^{-4} M). Measurement of the charge passed indicated that the total charge in both cases was identical, at least within experimental error. However, in the case of the en-silane electrode, the magnitude of the 618 eV band is much larger than for that band on the pr-silane modified electrode.

There are two possible explanations which can be supported by the data. The first assumes different molecular surroundings of the dye at the electrode surface and of the dye layers on top of this. The second assumes the production of molecular iodine or iodide ion at the electrode surface, covered with overlayers of adsorbed dye.

If it is assumed that the dye is electrochemically adsorbed in a layer-on-to-of-layer fashion, results like those mentioned above might be expected. Those dye molecules at or close to the chemically modified electrode surface would be expected to be in a different molecular environment than those molecules making up the successive overlayers. Therefore, it would be expected to see a small shift in binding energies for the molecules in different environments. However, shifts as large as observed on the modified surfaces (3 eV) would not be expected. Further, a similar phenomenon is not observed for the case of unmodified (clean) tin oxide, as might be expected based on the same above discussion.

The second explanation, the formation of either I_2 or I^- at the electrode surface, is based on several previous observations. The reported binding energies for iodine (I_2) and Iodide (I^-) are 618.0 eV, exactly as observed on the pr-SnO_2 and en-SnO_2 electrodes. However, the presence of I_2 or I^- would require the displacement of an iodine molecule for the dye, as might occur by neucleophilic attack.

It is known that a thiol can displace iodine bound to either aromatic or aliphatic molecules, forming a carbon-

sulfur bond, with the resulting liberation of HI (50,51). Nitrogen, in the form of an amine, is also a good nucleophile; therefore, it is conceivable that the same reaction could occur. Further, there is some precedent for the electrochemical displacement of iodine by nitrogen (52,53). Miller and Hoffman (54) have observed this displacement of iodine from alkyl iodides, at platinum, via a carbonium ion intermediate:

$$R\text{-}I \xrightarrow{(-e^-)} R^+ + 1/2\ I_2$$

$$R^+ + CH_3CN \longrightarrow R\text{-}N = C^+\text{-}CH_3$$

$$R\text{-}N = C^+\text{-}CH_3 = H_2O \longrightarrow$$

$$CH_3\text{-}\underset{\underset{O}{\|}}{C}\text{-}NH\text{-}R$$

This reaction proceeds at potentials near the anodic limit for platinum, +1.9 to 2.1 volts, as measured against a saturated calomel reference. Further, the reaction is not observed for alkyl bromides or alkyl chlorides. For conjugated systems where resonance stabilization can occur, such a reaction is possible. A possible mechanism might be:

$$R - I \xrightarrow{(-e^-)} R^+ + 1/2\ I_2$$

$$R^+ + :NH_2R' — (S) \longrightarrow R\text{-}NHR' — (S)$$

(R = dye, (S) = substrate)

In order to test this proposal, a number of experiments were performed, which were aimed at either proving or disproving it.

To test the effect on the peak potential using a different neucleophilic group, the same electrochemical adsorption was investigated using mercaptopropyltrimethoxysilane-modified SnO_2 (SH-silane). Figure 15 shows a series of cyclic voltammagrams, done at various dye concentrations, on mercaptosilane-modified tin oxide. At high concentrations (5.0×10^{-4} M), the anodic peak appeared again to be made up of two distinct processes occurring at potentials near to each other. Estimating that the peak potential for the more anodic process is at .825 volts vs. Ag^+ / AgCl, we see that this potential is very near than for pr-SnO_2 electrodes ($V_{peak} = 0.810$ volts: Figure 12). Varying the concentrations of these two peaks, however, does not vary the relative intensities of these two processes, as occurred in the pr-silane modified electrode case. However, the obvious cathodic shift would be expected in the presence of a better electron-doner, which the thiol is. Hence, it should be easier to produce the carbonium ion intermediate in the proximity of the electrode surface, because of a reduction in the activation energy. ESCA analysis for an SH-silane electrode with the electrochemically adsorbed erythrosin (1.0×10^{-4} M) was inconclusive. The appearance of two peaks for either the iodine $3d_{3/2}$ or $3d_{5/2}$ bands could not be detected due to poor signal-to-noise ratio caused by a

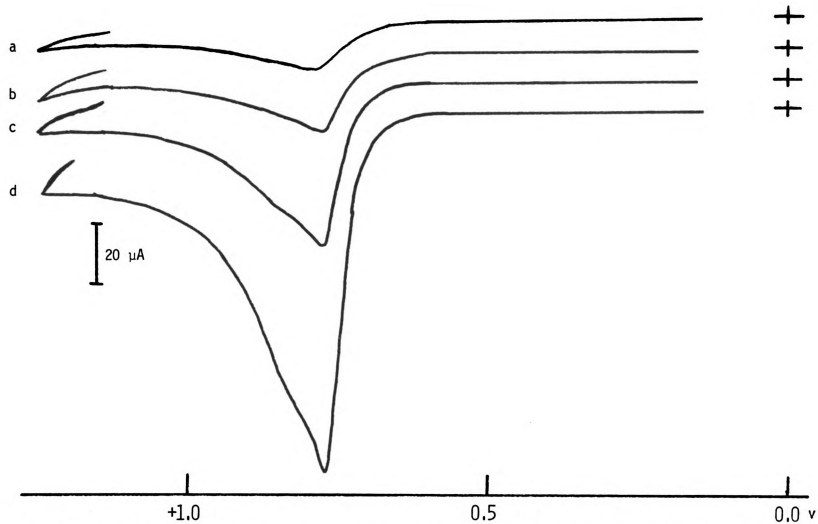

Figure 15. Cyclic voltammetry of Erythrosin at SH-silane modififed tin oxide; a = 5.0×10^{-5} M, b = 1.0×10^{-4} M, c = 2.5×10^{-4} M, d = 5.0×10^{-4} M; scan rate = 11.5 mv/sec.

rapidly deteriorating anode.

The next experiment performed involved the investigation of the unhalogenated form of erythrosin, fluorescein (see Figure 8), and eosin, a tetrabrominated form of fluorescein. These dyes were investigated at pr-silane, SH-silane and clean tin oxide electrodes. The cyclic voltammetry of these dyes on pr-silane modified electrodes are shown in Figure 16.

On pr-silane modified electrodes, rhodamine B no longer has an anodic peak, contrary to its behavior on clean tin oxide. Further, fluorescein (Figure 16a), shows only a slight increase in background current, which could be caused by IR drop across the SnO_2 and across the cell. Eosin, however, under identical conditions of linear potential scan, does show an anodic peak at 0.895 volts as measured against a silver/silver chloride reference. This is a shift of 80 millivolts more anodic than erythrosin, which is shown in Figure 14d. For eosin, the total charge passed is also 40% less than for erythrosin at the same concentration.

The behavior is identical to that expected. Bromine, being a poorer leaving group than iodide, would cause an anodic shift relative to iodine. It should require more energetic conditions to produce a carbonium ion where bromide is a substituent. On the basis of the electrochemical and ESCA data presented, as well as visual observations, the possibility of neucleophilic attack, with the loss of an iodine molecule, is conceivably possible.

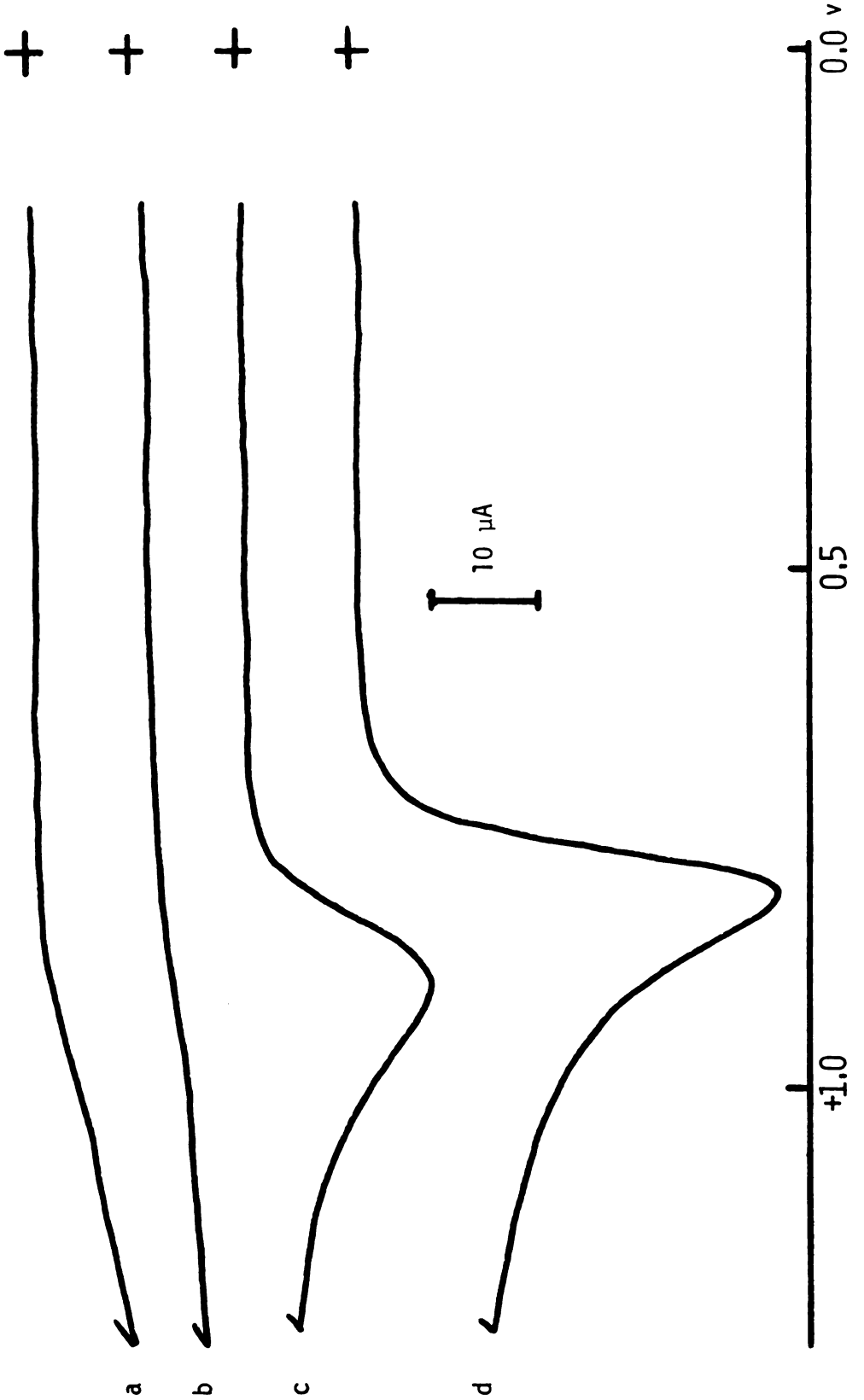

Figure 16. Cyclic voltammetry of various dyes on pr-silane modified tin oxide. All dyes 5.0×10^{-4} M in pH 7 buffer; a. Fluorescein, b. Rhodamine B, c. Eosin, d. Erythrosin. Scan rate = 11.5 mv/sec.

Figure 17 represents the speculated behavior for deposition of erythrosin on both clean and pr-silane modified tin oxide electrodes. For clean tin oxide surfaces, the first layer of deposited dye is in the form of the native dye. ESCA analysis verify this to be the case, which is indicated as Type I erythrosin in the associated Figure. At silane-modified electrodes, however, the first layers of adsorbed dye are of a form different than native erythrosin, indicated as Type II. Successive adsorbed overlayers are considered to be Type I. We assumed that the Type II dye was deposited at the electrode surface, since increasing the charge passed on the adsorption step (and hence the number of adsorbed monolayers), caused such a drastic reduction in ESCA signal intensity for this 618 eV binding energy component. The above model, however, may be somewhat misleading, as it assumes that continuous layers of either the Type I or Type II dye are deposited. It is equally possible, due to the surface irregularities of the vapor deposited SnO_2 layer, that the same phonomenon may be occurring in separate islands on the electrode surface.

Assuming that each erythrosin molecule lies flat on the surface, we calculated that each dye molecule should occupy 90 square angstroms. Therefore, there should be approximately 1.1×10^{-14} molecules/cm^2. Based on a one-electron process for the adsorption, and an electrode area of 0.636 cm^2, 11.3 microcoulombs of charge should be passed for every monolayer of adsorbed dye. Assuming further that all

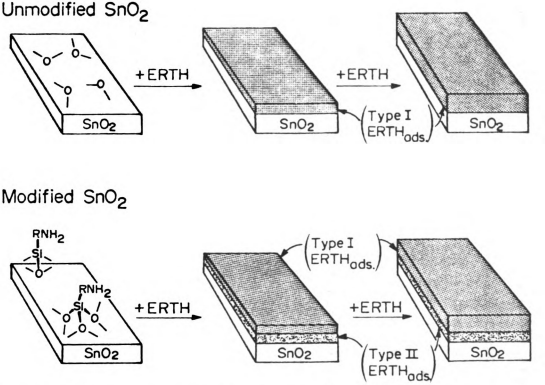

Figure 17. Observed behavior for dye electrochemically adsorbed on clean and silane-modified SnO_2 surfaces.

adsorbed layers of dye remain on the surface (not likely), the total number of adsorbed monolayers can be calculated knowing the charge passed. The results of such calculations are shown in Table 2.

For the deconvolved spectra, the iodine-to-tin ratios for the iodine $3d_{5/2}$ and sin $3d_{5/2}$ bands are also shown. All ratios are corrected for the differences between the relative cross sections for both elements (55). Those entries labelled with either (1) or (2) indicate the appropriate iodine-to-tin ratios for the particular binding energy components.

The values reported in the Table are also compared to those values for a sample of physically adsorbed erythrosin, and an electrochemically adsorbed sample of erythrosin on SH-silane modified SnO_2.

Accompanying Table 2 is Figure 18, which shows the equivalent monolayers of adsorbed dye plotted against the particular component iodine-to-tin ratios and total iodine-to-tin ratios. The apparent gradual increase in iodine-to-tin ratio for the 618.0 eV binding energy band also indicated that the relative amounts of Type II dye produced at the electrode surface remained almost constant, even though the number of monolayers adsorbed increased rapidly.

Table 2. Iodine to Tin Ratios and Binding Energies for Electrochemically and Mechanically Adsorbed Dyes

Sample	Approximate Monolayers	N_I/N_{Sn} [a]	Binding Energy (eV) [b]
Electrochemically adsorbed on clean SnO_2 (dye) = 2.5×10^{-4} M	20.3	28.2	620.1 ± 0.2
Electrochemically adsorbed on pr-silane/SnO_2 (dye) = 5.0×10^{-5} M	10.1	2.44	
		1.49 (1)	618.0 ± 0.2 (1)
		0.95 (2)	620.2 ± 0.2 (2)
Same as above (dye) = 1.0×10^{-4} M	20.0	5.08	
		0.80 (1)	618.4 ± 0.2 (1)
		4.28 (2)	621.0 ± 0.2 (2)
Same as above (dye) = 2.5×10^{-4} M	29.3	30.4	
		6.47 (1)	618.1 ± 0.2 (1)
		24.0 (2)	620.1 ± 0.2 (2)

Table 2 (cont'd.).

Sample	Approximate Monolayers	N_I/N_{Sn} [a]	Binding Energy (eV) [b]
Electrochemically adsorbed on pr-silane/SnO_2 (dye) = 5.0×10^{-4} M	49.9	80.8	
		9.44 (1)	618.6 ± 0.2 (1)
		71.3 (2)	621.2 ± 0.2 (2)
Electrochemically adsorbed on en-silane/SnO_2 (dye) = 2.5×10^{-4} M	29.3	49.3	
		15.4 (1)	618.0 ± 0.2 (1)
		33.9 (2)	620.6 ± 0.2 (2)
Electrochemically adsorbed on SH-silane/SnO_2 (dye) = 5.0×10^{-5} M	6.3	9.17	621.0 ± 0.2
Dye physically adsorbed on clean SnO_2	less than one	0.06	620.5 ± 0.2

[a] Corrected for known molecular cross-section differences.(55)

[b] Referenced to Sn $3d_{5/2}$ band at 486.2 eV.(12)

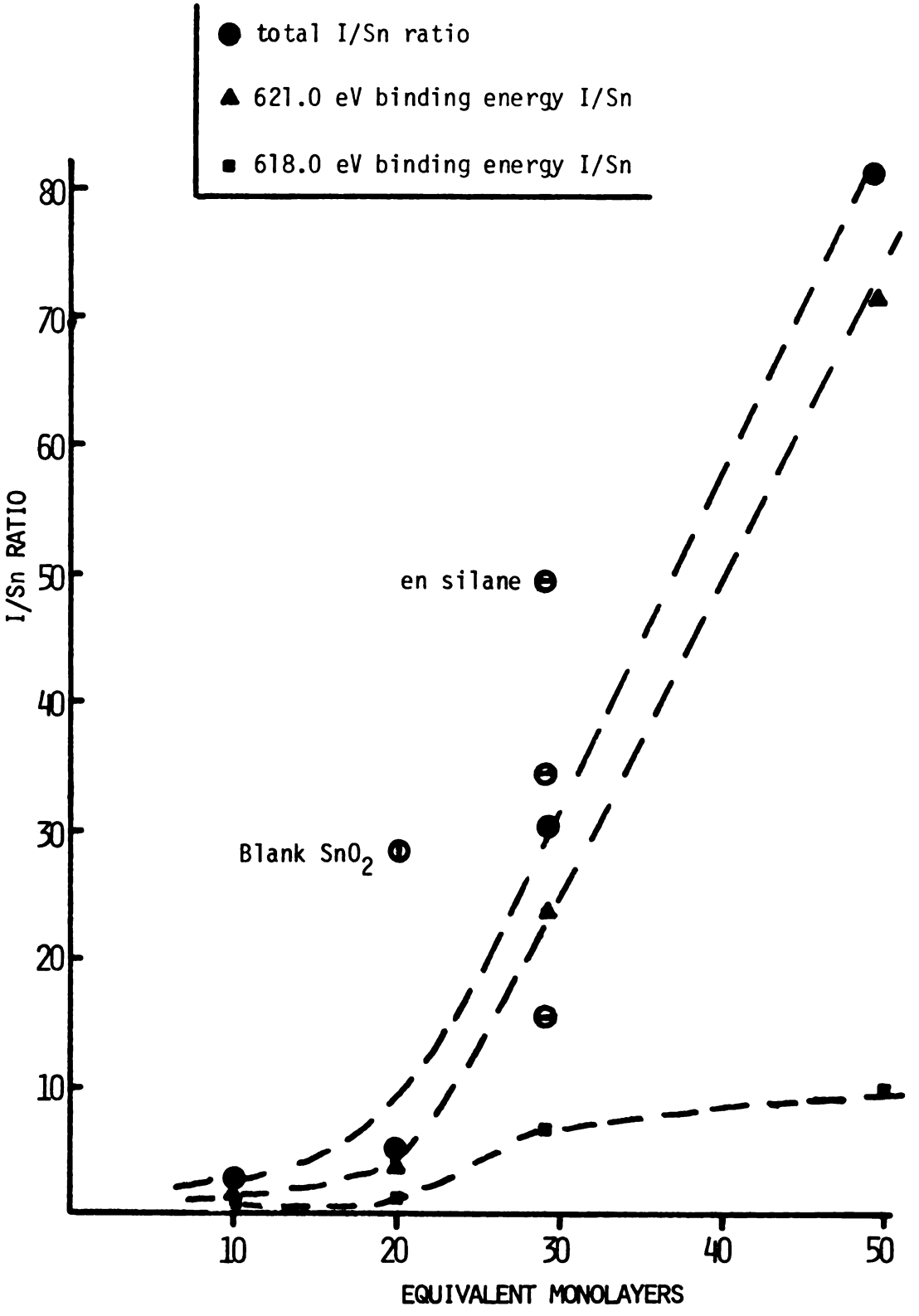

Figure 18. I/Sn ratios for electrochemically adsorbed dyes.

C. Electrochemical Characterization of Dye Adsorbed Surfaces Using the Electrochemically Reversible Ferro/Ferricyanide Couple

For the determination of effective electrode areas and to determine how electron transfer between the electrode and the solution is affected by overlayer formation, the ferrocyanide ($Fe(CN)_6^{3-}$ oxidation was studied. The kinetics of the ferri/ferrocyanide oxidation at SnO_2 electrodes are well understood (56). The solutions used were pH 4 buffer, which were 1.0 millimolar in potassium ferrocyanide. Electrode areas were determined chronoamperometrically using the Cottrell equation:

$$it^{1/2} = nFAC^{\cdot}(D/\pi)^{1/2}$$

The diffusion coefficient for ferricyanide ion is given as 6.30×10^{-6} cm^2/sec (56). Rearranging this equation to solve for A, we arrive at the proper form of the equation for determining the electrode area:

$$A = (it^{1/2})/nFC \cdot (\pi/D)^{1/2}$$

The symbols shown have the usual meanings:

n = number of electrons involved in the oxidation process per molecule oxidized,

F = Faraday constant,

C = solution concentration, expressed in $moles/cm^3$.

Figure 19 shows a series of cyclic voltammagrams on clean tin oxide electrodes which have been previously treated by electrochemical adsorption of erythrosin at varying concentrations. All electrodes were rinsed briefly with

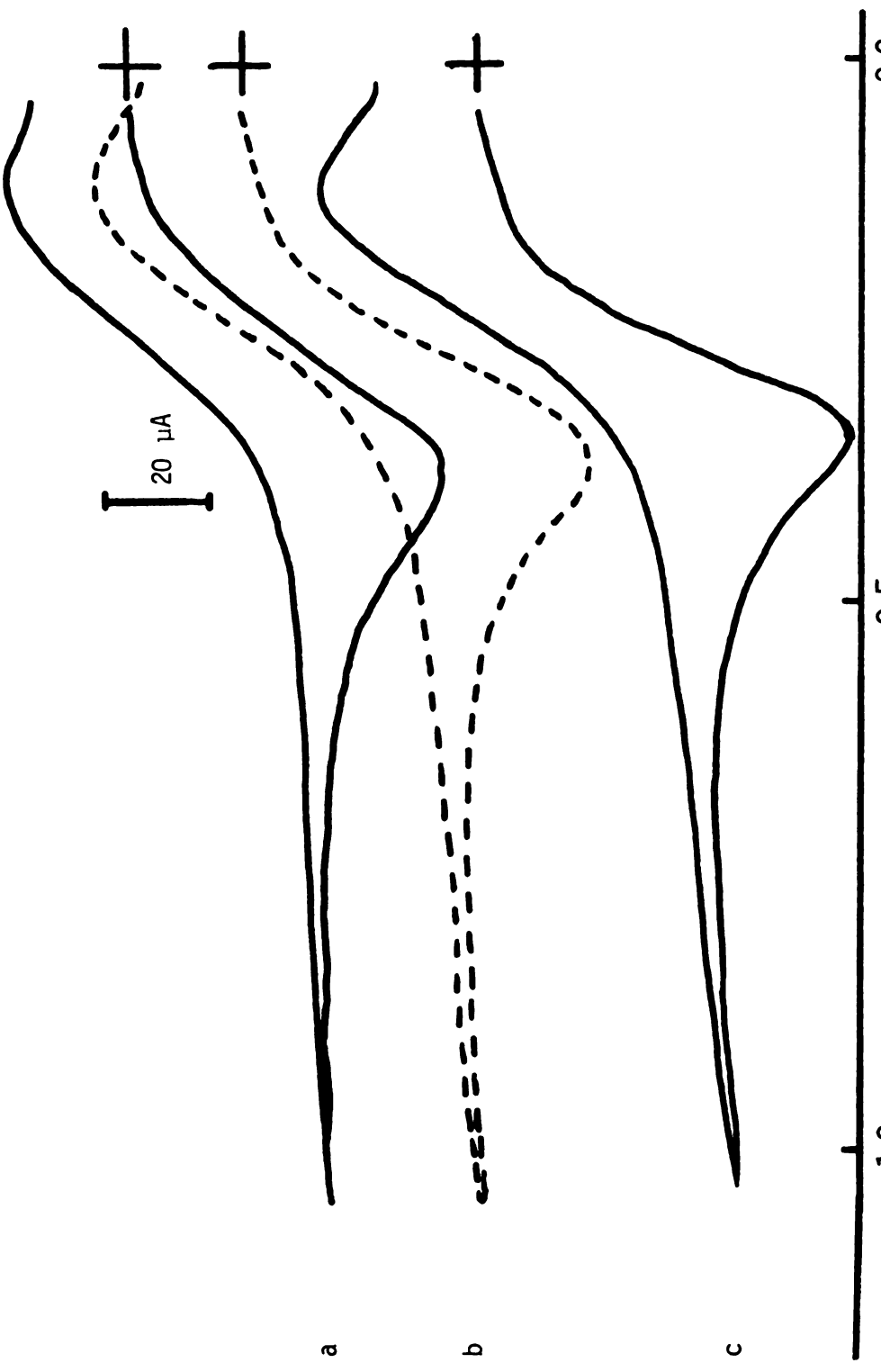

Figure 19. Cyclic voltammagram of ferri/ferrocyanide on unmodified SnO_2 after electrochemical adsorption of dye at various concentrations; a = 4.88×10^{-4} M, b = $.98 \times 10^{-4}$ M, c = 4.88×10^{-5} M.

distilled water after the electrochemical treatment, in order to remove any loosely held dye.

There is little effect on the peak potential separation of the redox couple with varying concentration of adsorbed dye, as is apparent from the Figure. There is apparently little retention of the dye at the electrode surface since there is almost no increase in the peak potential separation ($\Delta Ep = E_{peak}$ anodic - E_{peak} cathodic) with increasing number of monolayers of adsorbed dye.

Figure 20 shows a series of cyclic voltammagrams of ferrocyanide on pr-silane modified electrodes after undergoing dye adsorption at various concentrations. Figure 20c, with the lowest concentration of adsorbed dye, shows little difference in the peak potential separation from that for a pr-silane electrode before dye adsorption. At the highest adsorbed dye concentration, shown in Figure 20a, there is significant reduction of the peaks for either half of the redox couple, but a significant increase in background charging current. This behavior indicates that the electrode is largely blocked off to electron transfer.

A similar phenomenon is observed for SH-silane modified electrodes, as shown in Figure 21. However, in this case there is little concentration effect, unlike that observed for pr-silane electrodes. Even at the very lowest concentration investigated (1.0×10^{-5} M), both the oxidation and reduction waves were severely depressed, accompanied by a significant increase in background current, presumably due

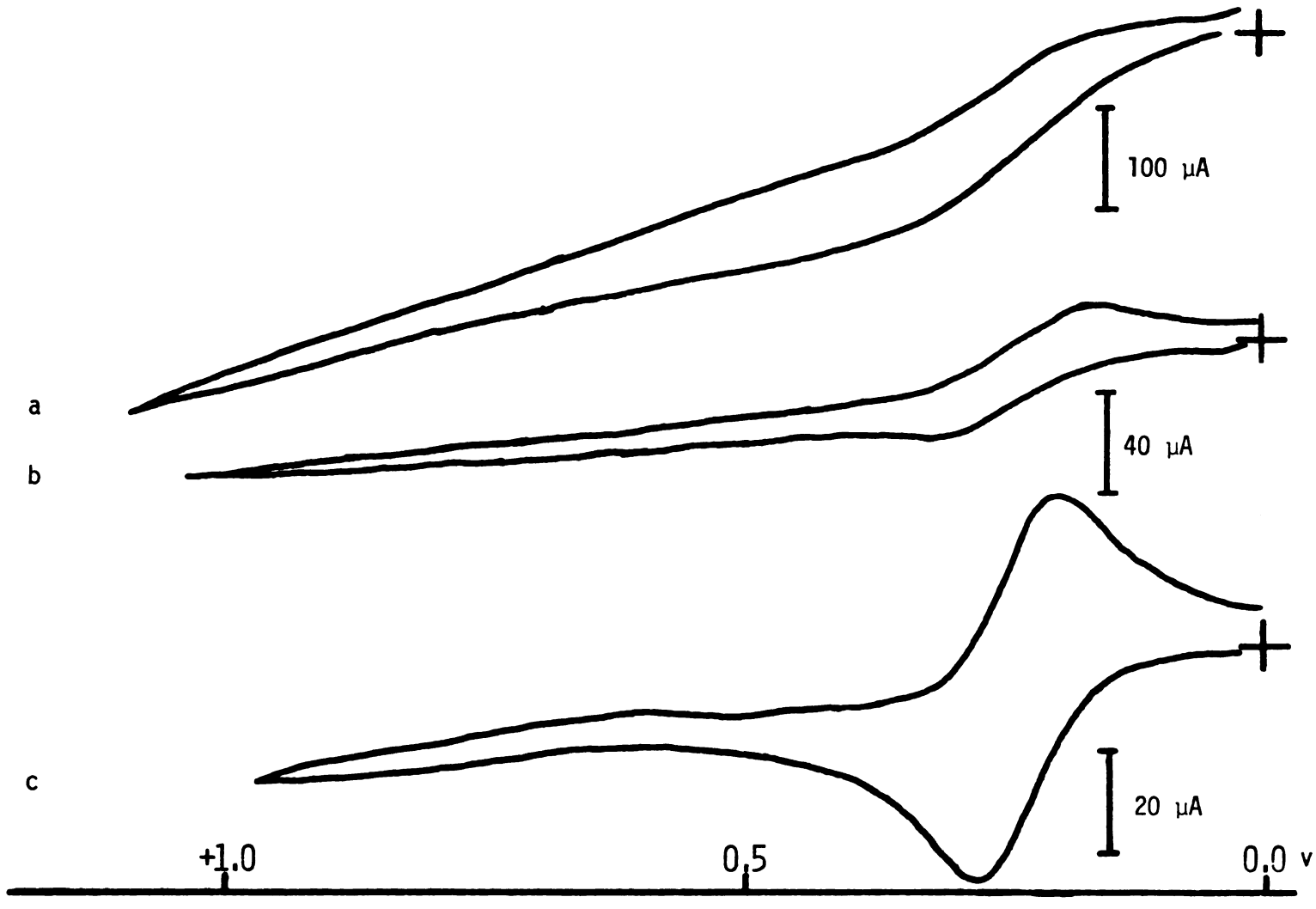

Figure 20. Cyclic voltammagrams of Ferrocyanide solution at α-aminopropyl silane modified tin oxide electrodes after electrochemical adsorption of dyes at various concentrations; a = 4.88×10^{-4} M, b = $.98 \times 10^{-4}$ M, c = 4.88×10^{-5} M.

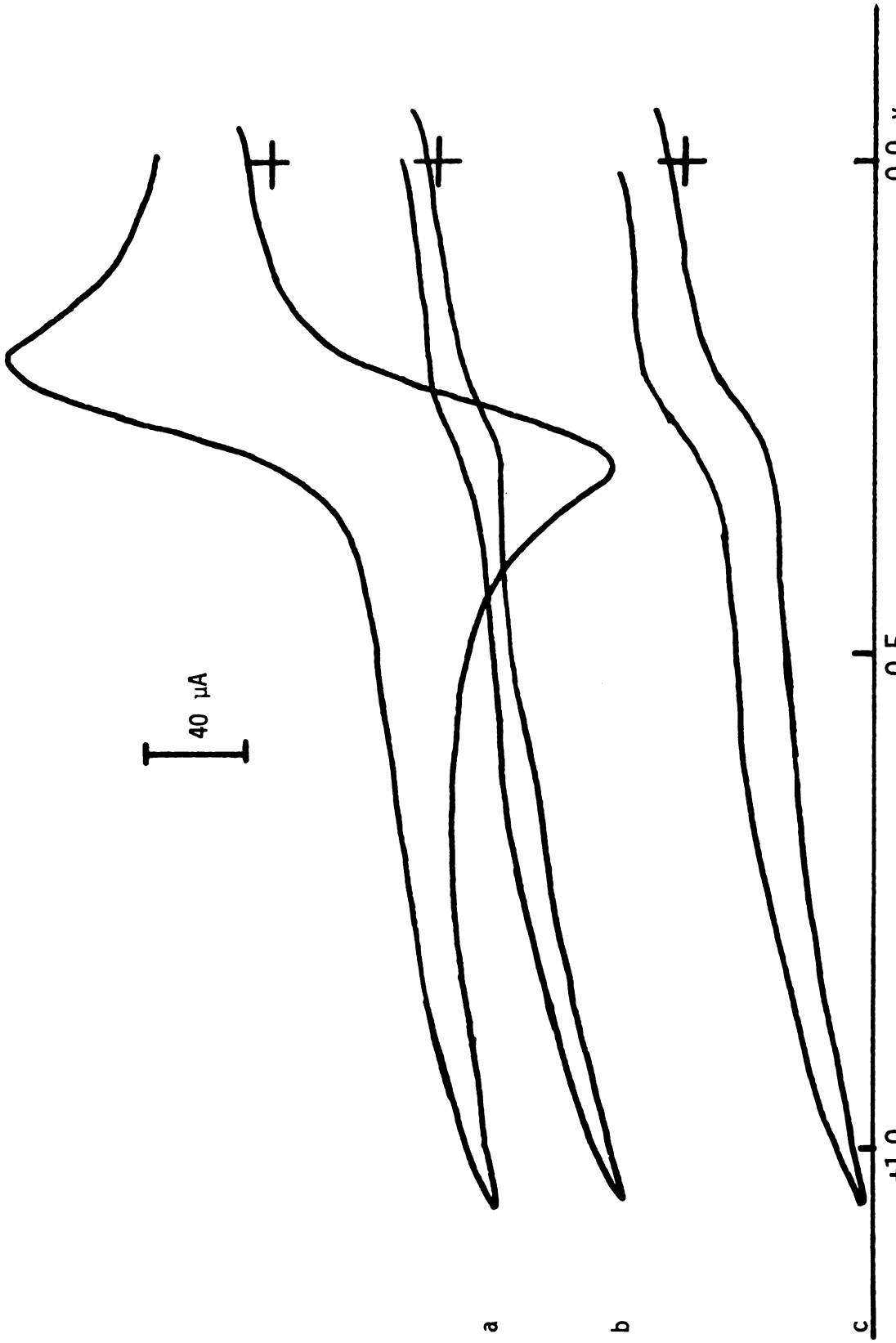

Figure 21. Cyclic voltammagrams of 1.0 mM Ferrocyanide solution at mercaptopropylsilane modified tin oxide electrodes before and after electrochemical adsorption of dyes at various concentrations. a. SH-SnO_2 electrode, b = 4.88 x 10-4 M, c = .98 x 10-4 M. Scan rate = 11.5 mv/sec.

to double-layer charging effects. However, there are two distinct breaks in the cyclic voltammagram at all concentrations, indicating that the redox process is still occurring at the electrode surface.

Determination of the effective electrode area for each type of modified surface also provided some interesting information. A summary of the data is given in Table 3. Also provided in this Table are values for the charge passed on each electrochemical dye adsorption, along with the concentration of the dye in solution for which the electrochemical adsorption was performed. ΔE_{peak}, the peak potential separations for the redox couple ferri/ferrocyanide are also given. Values of this particular parameter are also given before the adsorption step. Since the chronoamperometric data did not give the correct values for electrode area due to cell configuration, all values were scaled to the known geometric area, 0.636 cm^2.

For unmodified tin oxide, chronoamperometric data showed only a 15% reduction in effective area between the clean surface and that modified by adsorption at the lowest concentration (5.0×10^{-5} M). After this initial reduction, only a small decrease was observed with increased concentration. An apparent reduction in electrode area is also observed in the case of pr-silane modified electrodes after the dye adsorption. Similar to the behavior observed on clean tin oxide, there is only a small decrease in electrode area between the pr-silane electrode surface and the dye

Table 3. Electrochemical behavior of Tin Oxide Surfaces With Adsorbed Dye Layers.

Sample	(dye) M	Charge (microcoulombs)	A_{eff} (cm^2)	E_{peak} (mv)
clean SnO_2	0 (blank)	———	0.636[a]	105
clean SnO_2	5.0×10^{-5}	70.5	0.641	105
clean SnO_2	1.0×10^{-4}	102.6	0.622	110
clean SnO_2	2.5×10^{-4}	347.9	0.572	105
clean SnO_2	5.0×10^{-4}	514.7	0.567	105
pr-silane SnO_2	0 (blank)	———	0.615	80
pr-silane SnO_2	5.0×10^{-5}	103.9	0.588	125
pr-silane SnO_2	1.0×10^{-4}	154.8	0.598	125
pr-silane SnO_2	2.5×10^{-4}	497.0	0.486	140[b]
pr-silane SnO_2	5.0×10^{-4}	742.0	0.323	225[b]

Table 3 (cont'd).

Sample	(dye) M	charge (microcoulombs)	A_{eff} (cm^2)	E_{peak} (mv)
en-silane SnO_2	2.5×10^{-4}	132.0	0.516	195
SH-silane SnO_2	0 (blank)	———	0.636[a]	95
SH-silane SnO_2	5.0×10^{-5}	237.5	0.521	100[b]
SH-silane SnO_2	1.0×10^{-4}	366.0	0.161	100[b]
SH-silane SnO_2	2.5×10^{-4}	787.0	0.134	100[b]
SH-silane SnO_2	5.0×10^{-4}	1676.0	0.119	100[b]

[a]Values scaled to known correct geometric area (0.636 cm^2) using indicated values.

[b]Estimated peak potential separation from cyclic voltammagram.

adsorbed surface (5.0×10^{-5} M). At the highest dye concentration, however, there is an almost 40% reduction in the area, which is accompanied by an increase in the peak potential separation for the redox couple.

For SH-silane modified tin oxide, the reduction in electrode area with increased dye concentration for the adsorption step is much more dramatic. For these electrodes, the quantity of charge passed for the dye adsorption step is at least 80% greater than for either the clean tin oxide or pr-silane modified surface. The ΔE_{peak} values remain almost unaffected.

Figure 22 shows a plot of $it^{\frac{1}{2}}$ against time for SH-silane electrodes after dye adsorption at various concentrations. Extrapolation of each series of points back to zero time gives the approximate value for area calculations. For the SH-silane electrodes with dye electrochemically adsorbed at low concentrations, there is only a small reduction in the time = 0 intercept. At higher concentrations, however, the $it^{\frac{1}{2}}$ values approach a lower limit.

This limiting behavior is also observed for pr-silane electrodes. Examination of Table 3 indicates that there is a sharp reduction in electrode area after about 250 microcoulombs of charge are passed. Based on earlier calculations, this represents about twenty equivalent monolayers of adsorbed material. Doubling the charge passed, and hence the number of adsorbed monolayers, has little effect on the electrode area after about the first twenty monolayers of dye have been adsorbed.

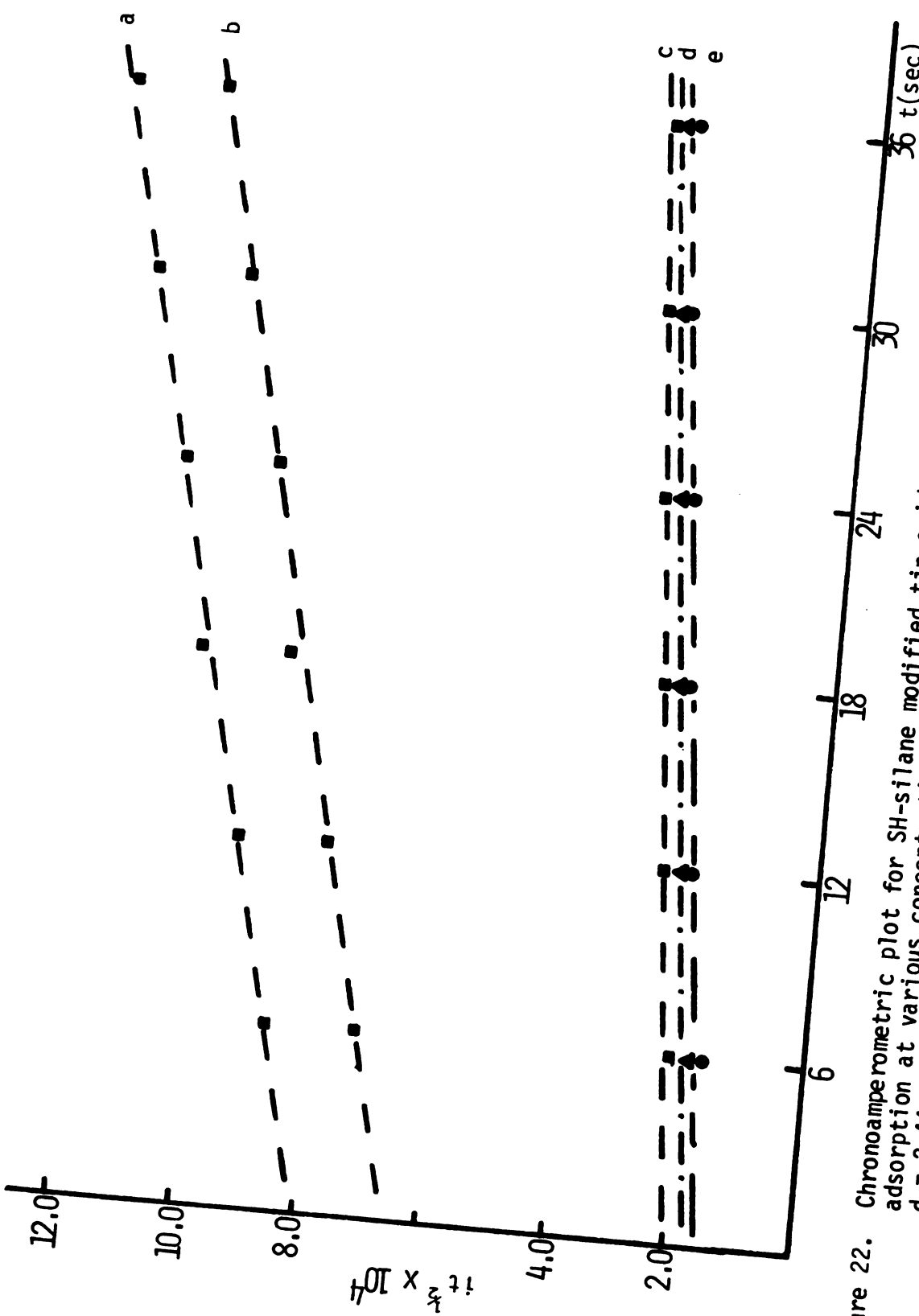

Figure 22. Chronoamperometric plot for SH-silane modified tin oxide before and after electrochemical dye adsorption at various concentrations; a = blank, b = 4.88 x 10-5 M, c = .98 x 10-4 M, d = 2.44 x 10-4 M, e = 4.88 x 10-4 M.

The apparent reduction in electrode area results in part by blocking of the electrode surface to electron transfer (56,57). The electrode area may be being blocked in part by islands of dye isolated on the surface. By examination of the equation for calculation of the area, it is apparent that a reduction in current values (i) will result in a decrease in area. The reduction in current can be accounted for by an increase in charging current for the electrode double layer, or by consumption of current in a second oxidative process at the electrode surface.

D. Covalent Attachment

Two methods of covalent attachment were investigated, one of which is novel to the covalent modification of semiconductor surfaces. The other, more conventional method, involves the formation of an amide bond.

The thiol attachment has been widely employed in the biochemical sciences for protein linkage or modification (50, 51). The kinetics of the thiol reaction are widely known. Figure 23 summarizes the reaction steps involved. The reaction proceeds rapidly at room temperature, in aqueous solutions at or near pH = 7. Chaiken and Smith (50) observed the kinetics of the reactions of the sulfhydroyl group of papain with chloroacetic acid, and found that the reaction is second order, proceeding by the following reaction:

$$ESH \xrightarrow{k_1} ES^- + H^+ \xrightarrow[RCl]{k_2} ESR$$

THIOL

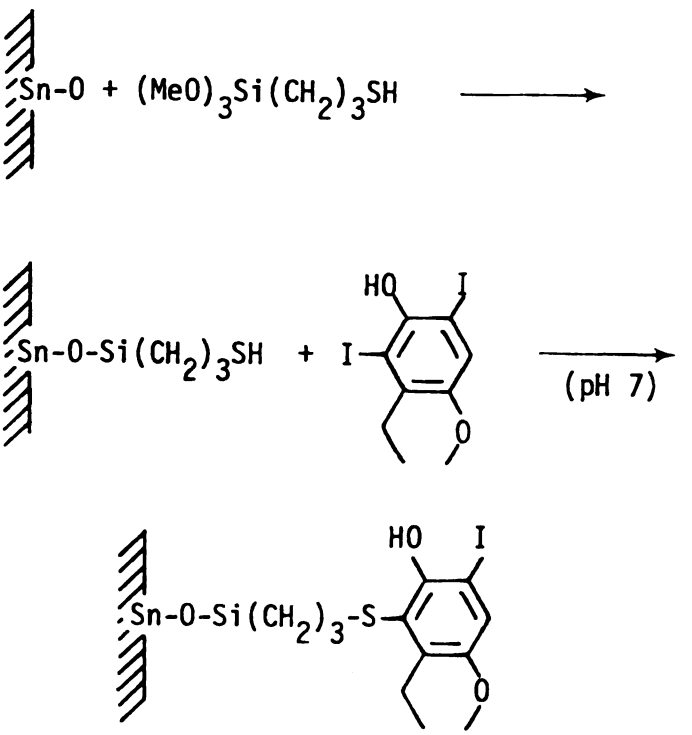

Figure 23. Reaction steps for Thiol attachment.

The rate constant for k_1 was found to be largest at pH = 5, while k_2 reached a maximum at pH = 6.

The dye-modified electrodes showed good retention of the dye, even after long periods of extraction in various solvents. Clean glass or tin oxide electrodes which had not been silane-modified quickly lost all evidence of dye retention upon extraction, however. Figure 24 shows a UV-Visible spectrum of the dye attached to clean glass, which was run using only the unmodified glass as a reference. The upper spectrum shows the dye-modified glass after being extracted twelve hours in ethanol. Calculation of the number of molecules per square centimeter, assuming a molar absorptivity of 130,000 $\underline{M}^{-1}$ cm^{-1}, gives approximately 4.0×10^{14} molecules-cm^{-1}. This number is about four times what would be expected for monolayer coverage, if the molecules were assumed to be lying flat on the surface. The second spectrum in Figure 24 shows the same piece of glass after a brief stripping with concetrated nitric acid. Note that the dye peak has completely disappeared.

A schematic for the amide attachment is shown in Figure 25. The reaction, commonly used in peptide synthesis and coupling reactions (58), produces an amide linkage with the resulting liberation of carbon dioxide. For the attachment, either en-silane electrodes or pr-silane electrodes were used. The accepted mechanism for the reaction using DCC, is shown in Figure 26 (59,60,61).

Like the mercapto-attached dye, electrodes modified in

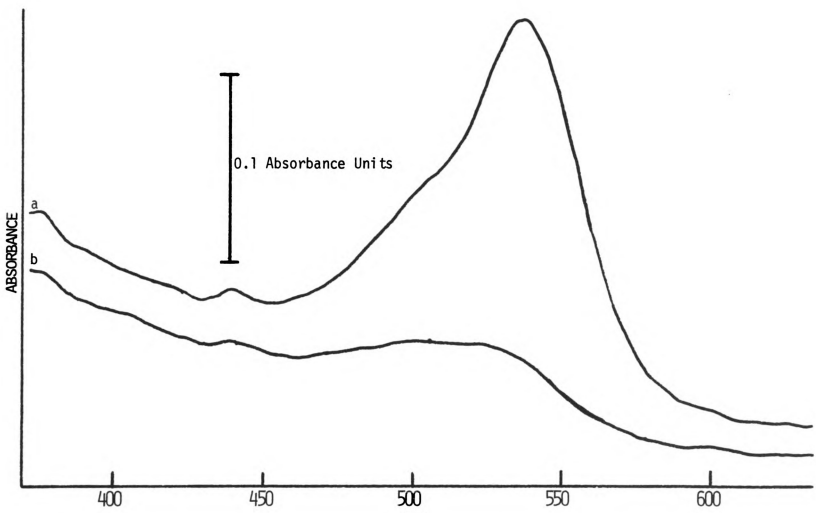

Figure 24. UV-visible spectrum of dye attached to glass by Thiol. a. dye-attached glass, b. glass after stripping.

AMIDE

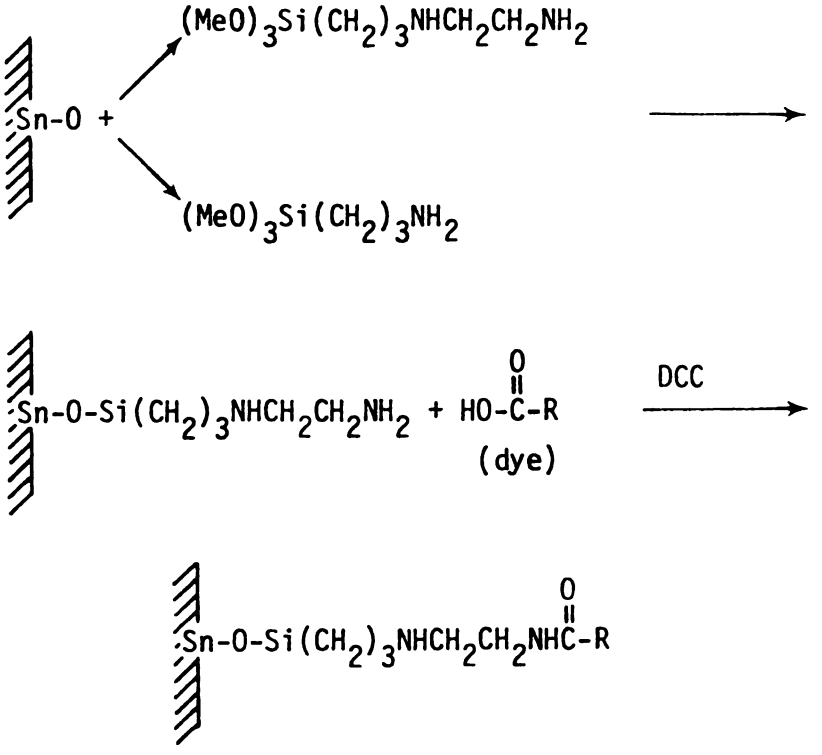

Figure 25. Reaction steps for Amide attachment.

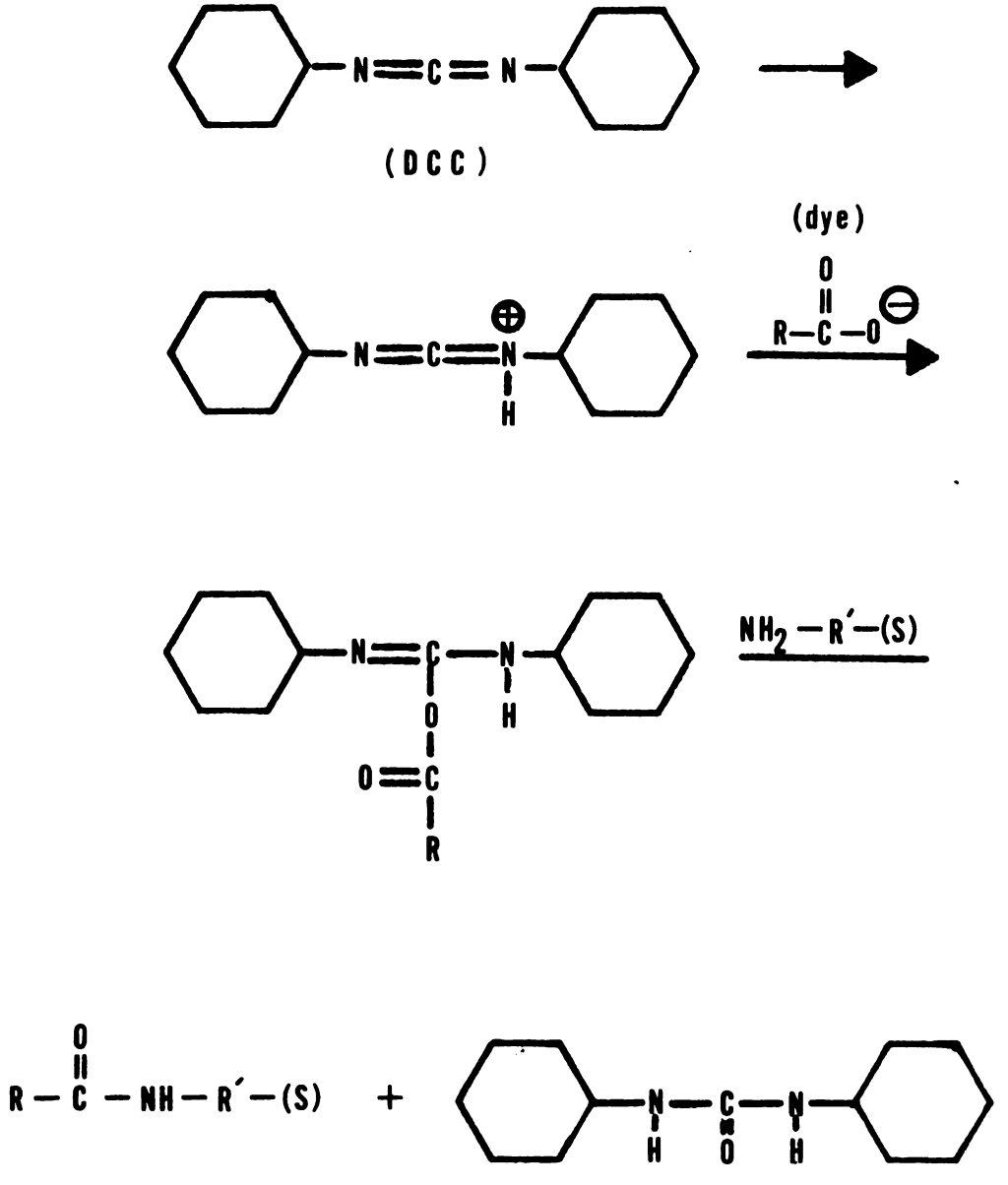

Figure 26. Mechanism for Amide attachment using dicyclohexyl-carbodiimide.

this manner could be extracted for extended periods of time without extensive loss of color. However, electrodes or glass which had not been previously silane-modified also retained small amounts of dye after the reaction, which could not be extracted. Therefore, it cannot conclusively be stated that this is a true covalent attachment. Rather, it may simply be the hydrophilic tendency of the dye to irreversibly adsorb to the electrode surface in a nonaqueous solution. There seems to be no evidence indicating the attachment should occur at unmodified tin oxide surfaces. The UV-Visible spectrum of a dye-attached tin oxide electrode is shown in Figure 27, both before (a) and after (b) a brief stripping with concentrated nitric acid. Note the similarity of spectrum (a) to that shown in Figure 21 and to the solution spectra shown in Figure 9, which confirms the presence of bound dye.

ESCA analysis of both forms of the bound dye verify the presence of dye at the electrode surfaces. There is little difference in the peak shapes for either the physically adsorbed dye or either of the methods of covalent attachment (Figure 28). Calculation of the I/Sn ratios for both cases gave .594 for mercapto attachment and approximately 1.0 for amide attached. Note the absence of two components in either iodine $3d_{3/2}$ or $3d_{5/2}$ bands, as was observed in the case of electrochemically adsorbed dyes on pr-silane modified electrodes. There is no apparent iodine or iodide at the mercapto-attached tin oxide surface, as would be

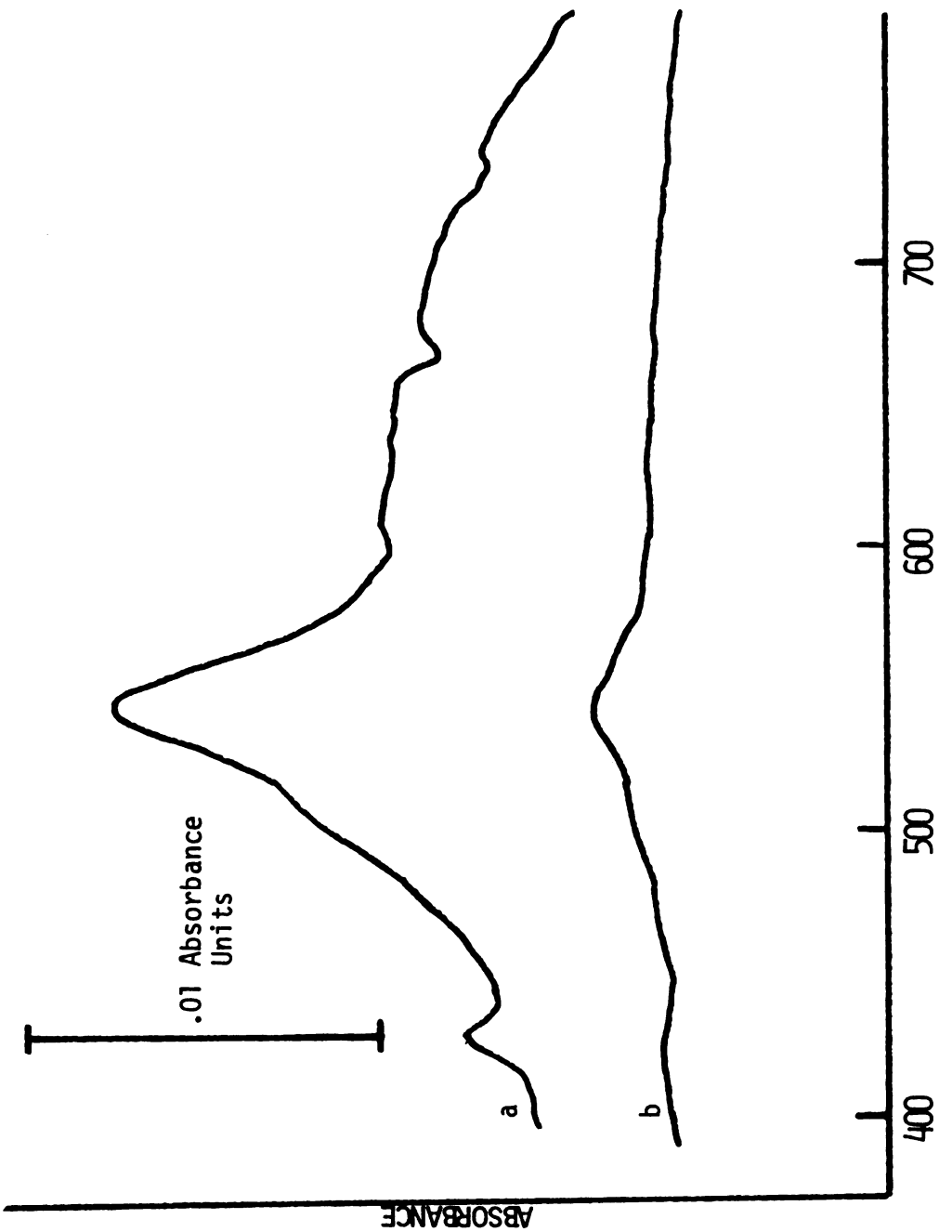

Figure 27. UV-visible spectrum of Erythrosin attached to amidization on en-silane modified tin oxide; a. dye attached, b. after stripping.

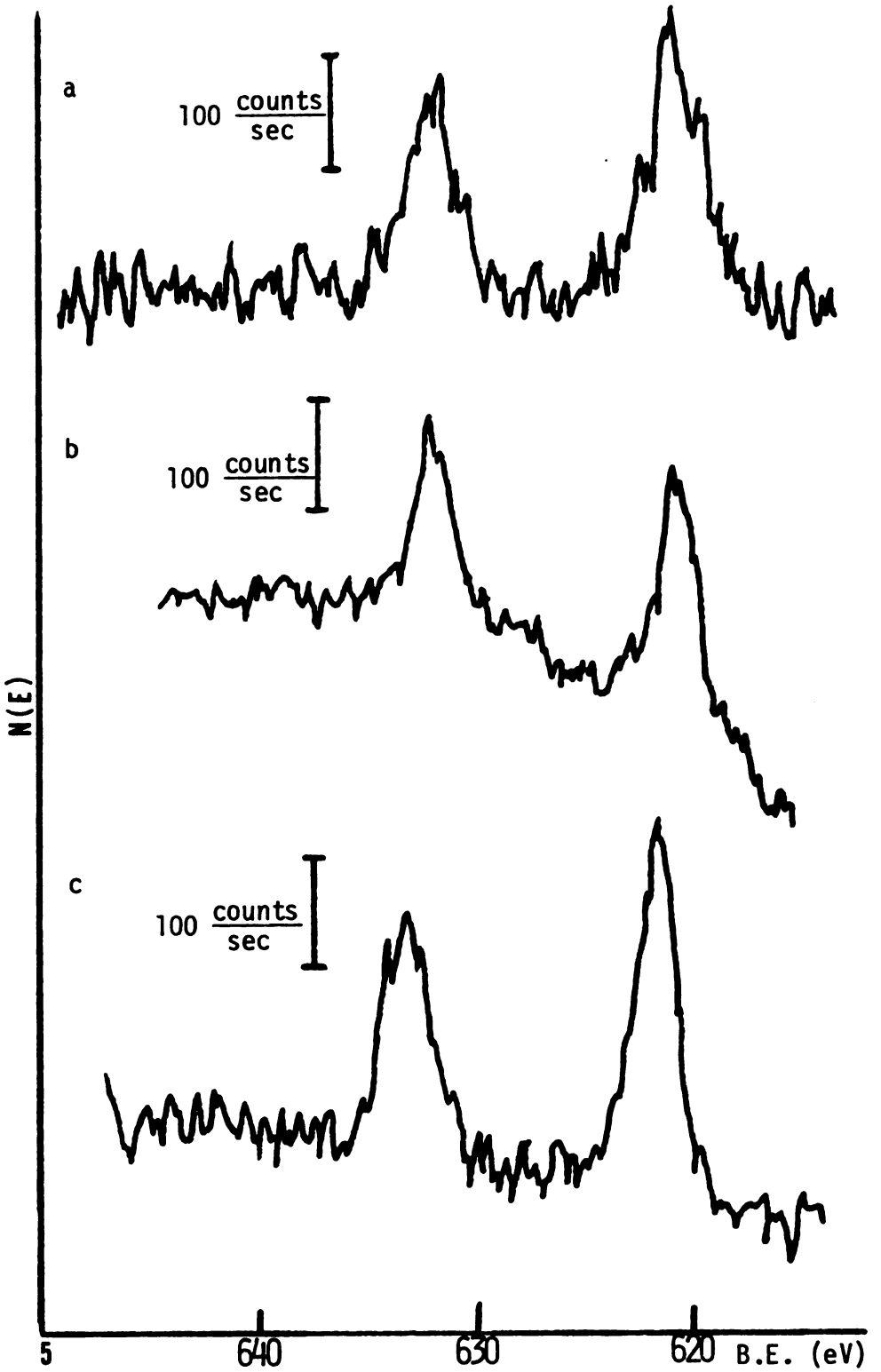

Figure 28. ESCA analysis of I $3d_{3/2}$ - $3d_{5/2}$ bands for mechanically adsorbed and covalently bound dyes; a. standard, b. Amide attached, c. Thiol attached dye

expected due to this method of attachment, indicating that most of the iodine liberated is easily extracted from the electrode surface.

Ferro/ferricyanide cyclic voltammagrams of the surface showed little effect on the electrode area, indicating that most of the surface was accessible to electron transfer. Examples of cyclic voltammagrams on tin oxide electrodes before and after dye attachment are given in Figures 29 and 30. Comparison of these results to those shown for electrochemically adsorbed dyes indicates little effect on the surface. Chronoamperometric data also showed little difference in the electrode area, again verifying that the surface area had been only slightly affected. However, the trends observed for both types of attachment are important. These results are summarized in Table 4.

Table 4. Chronoamperometric Data for Bonded Electrodes

Sample	$it^{\frac{1}{2}}$ (at t=0)	A_{eff} (cm^2)[a]
Clean SnO_2	7.45×10^{-5}	.545
SH-SnO_2	7.70×10^{-5}	.564
Dye - SH-SnO_2	8.00×10^{-5}	.586
en-SnO_2	8.50×10^{-5}	.622
Dye - en-SnO_2	8.29×10^{-5}	.607

[a]Using $D = 6.50 \times 10^{-5}$ cm^2/sec. (56)

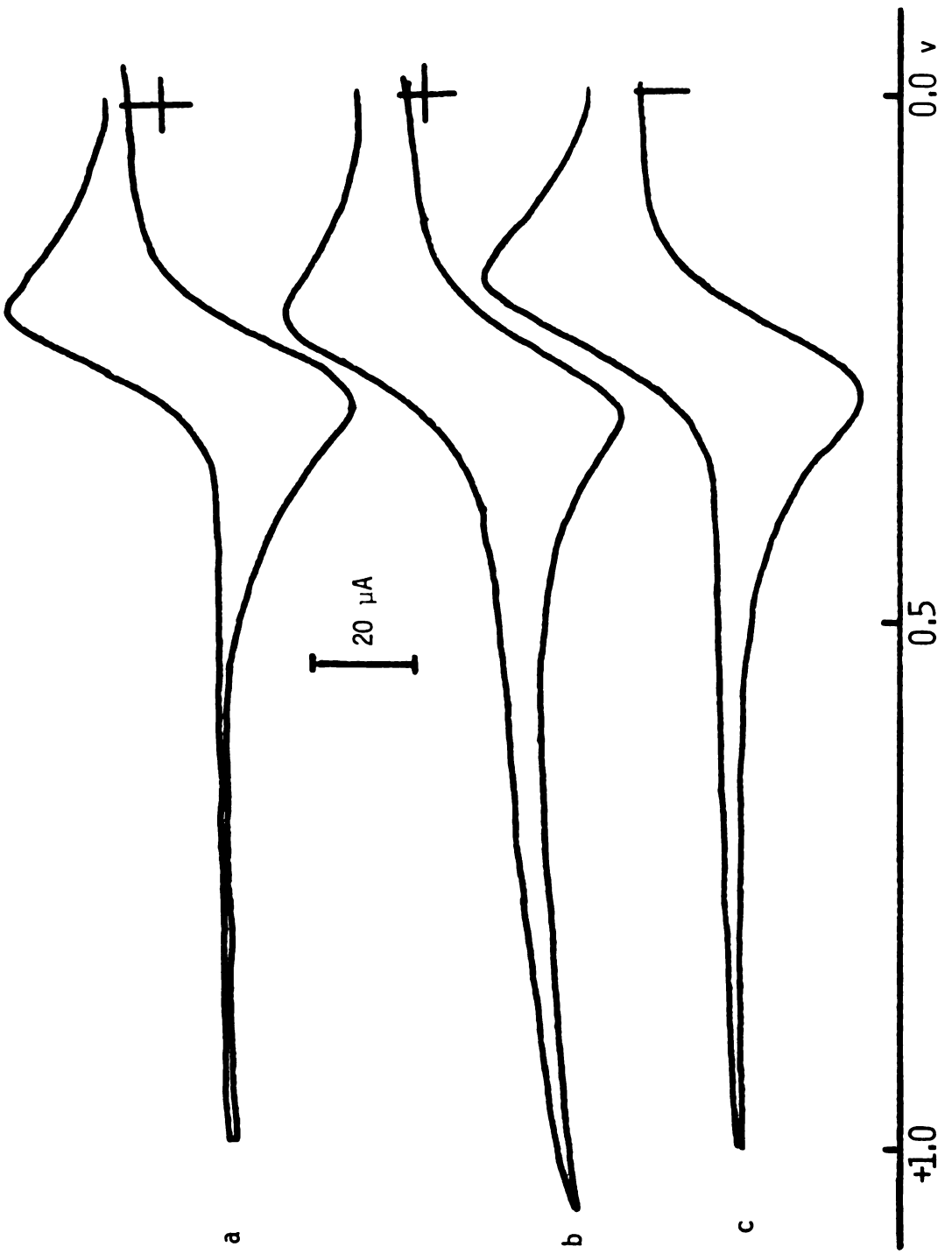

Figure 29. Cyclic voltammagrams of 1.0 mM ferrocyanide in pH 4 buffer after various stages of modification; a. clean SnO_2, b. mercaptosilane modified SnO_2, c. dye attached to SnO_2 by Thiol linkage. Scan rate = 11.5 mv/sec.

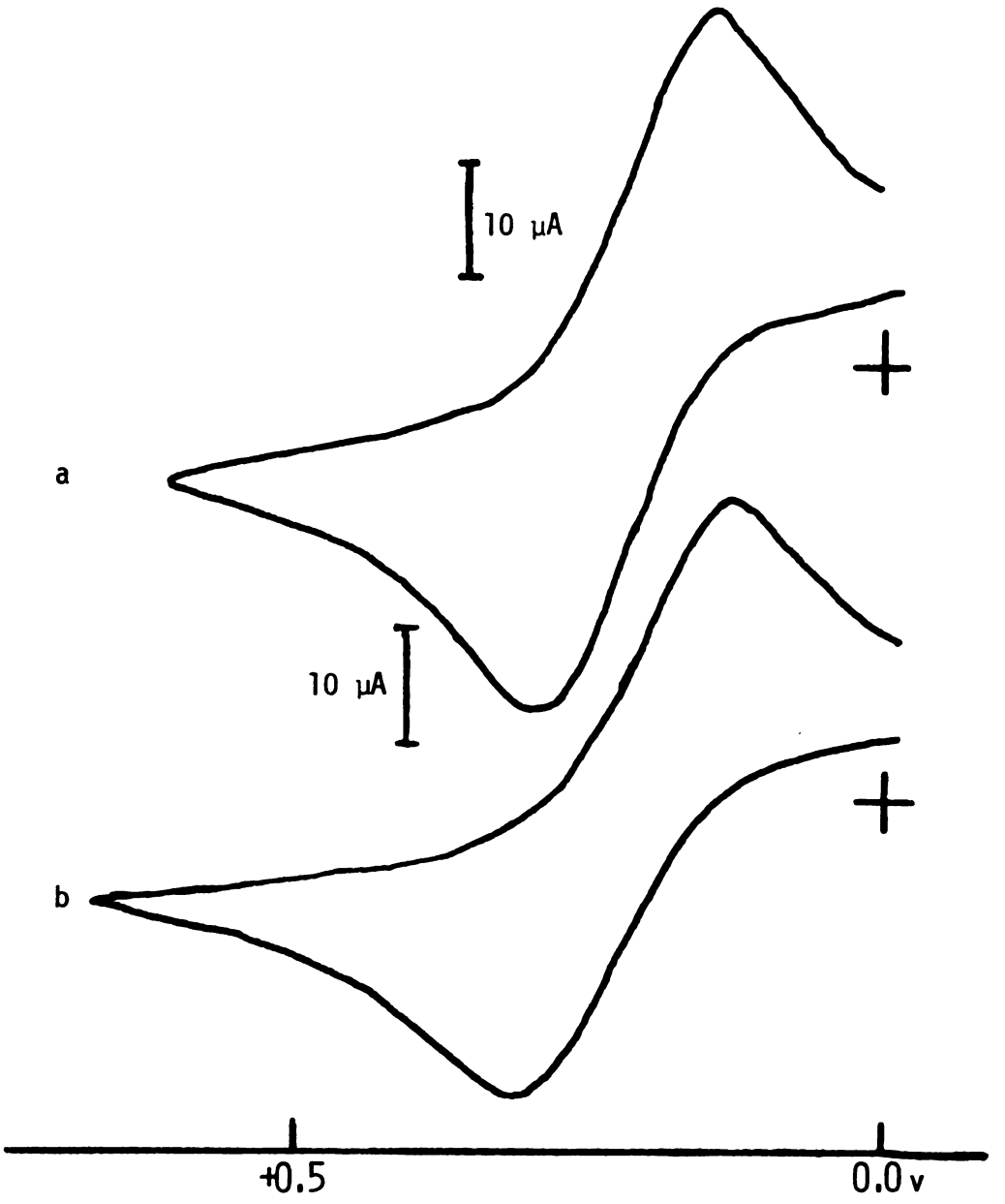

Figure 30. Cyclic voltammagrams of 1.0 mM ferrocyanide in pH 4 buffer after various stages of modification; a. en-silane modified SnO_2, b. dye attached to SnO_2 by amidization. Scan rate = 11.5 mv/sec.

In each case, the electrode area increased slightly after the electrodes were treated with the silane. After dye attachment, electrode area again increased, in the case of the thiol attachment, but was reduced for the amide. The observed trend may be caused by an increase in charging current after silane, with a further increase after dye attachment (thiol case).

Measurements of double layer capacitance in order to determine carrier density (n_0) and flatband potential also indicate two separate trends for the thiol and amide attachments. The slope, as measured from a plot of $(1/\text{capacitance})^2$ against bias potential (Mott-Schottky plot), is inversely proportional to carrier density.

$1/C^2$ vs potential plots for the thiol modified SnO_2 electrodes, shown in Figure 31, indicate only a small change in carrier density between clean and either form of the modified surface. The slight cathodic shift of the flat band potential for either modified case cannot be attributed entirely to changes in the space charge capacitance. In the case of a semiconductor, the Helmholtz capacitance is assumed to be much larger than the space charge capacitance, and also to be independent of potential (62). However, when the surface of these electrodes are modified, most of the major structural activity, and hence change, occurs within the outer Helmholtz plane. Therefore, the observed behavior cannot be attributed to changes in space charge capacitance alone.

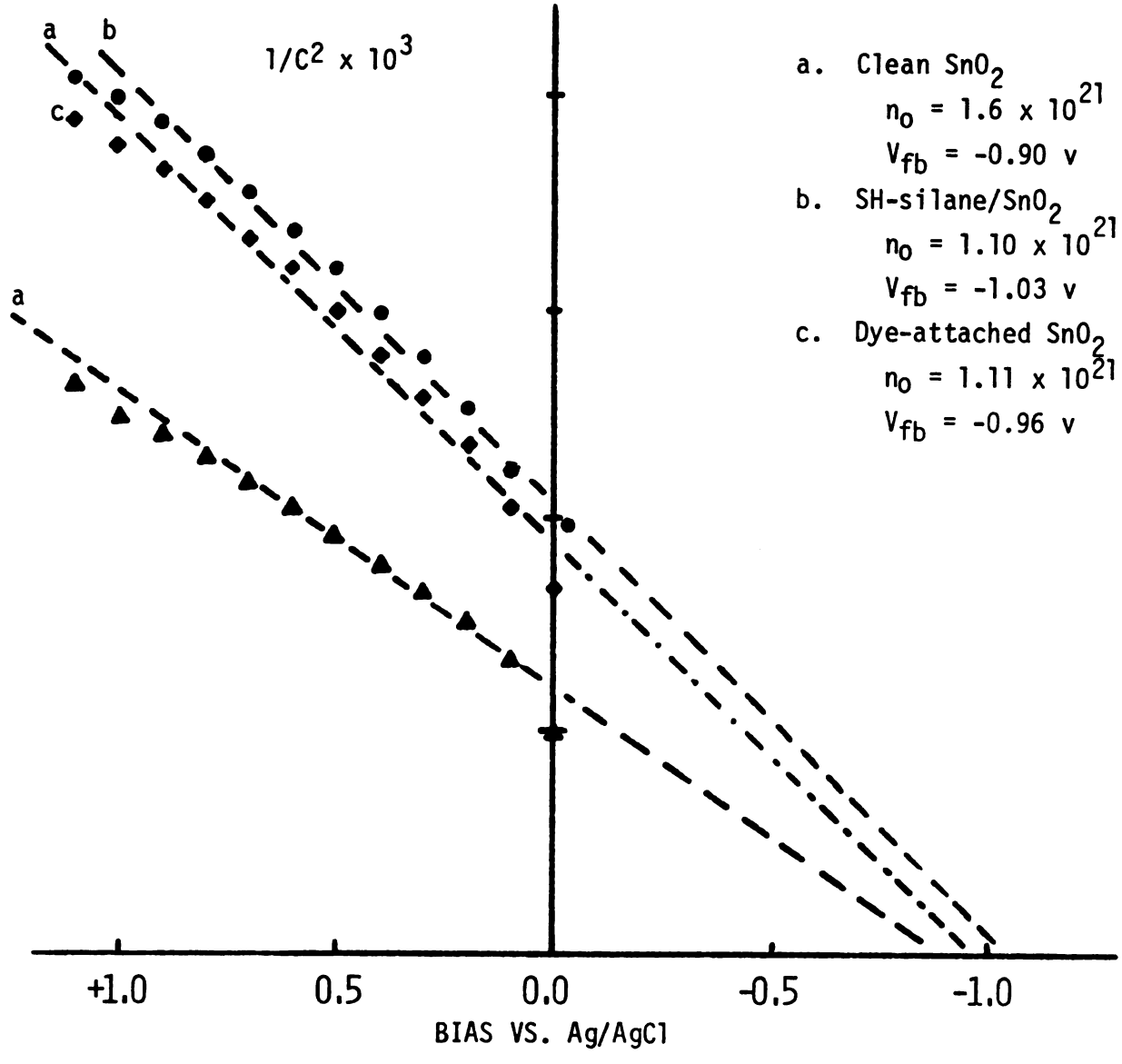

Figure 31. Mott-Schottky plot for dye attached to tin oxide by Thiol linkage.

An increase in the flat band potential indicates that the potential drop across the space charge region is larger at any applied potential, which requires that the potential drop across the Helmholtz layer is also greater. Addition of a nonconducting functionality to the electrode surface should give a greater potential drop across the Helmholtz region, consistent with the observed data.

Mott-Shottky behavior for amide attachment using pr-silane modified electrodes showed identical behavior to that for a mercapto attachment. In the case of en-SnO_2, however, there was a significant effect in both carrier density and flat band potential. This is consistent with the chemical behavior of those electrodes modified using the 3-(2-aminoethylamino)-propyltriethoxysilane (Figure 32). The silanization reaction is extremely difficult to control, and cross-polymerization is more possible. Therefore, the silane addition acts to add a significant insulating character to the electrode surface, causing a reduction in the carrier density. The visibly greater degree of dye attachment in the amide case at en-silene modified surfaces would act to further insulate the electrode surface, resulting in a greater potential drop across the Helmholtz region.

E. Photocurrent Measurement

The entire object of this research has been to observe photocurrent generation, and how it is enhanced by modification using either monolayer (covalent) or multilayer

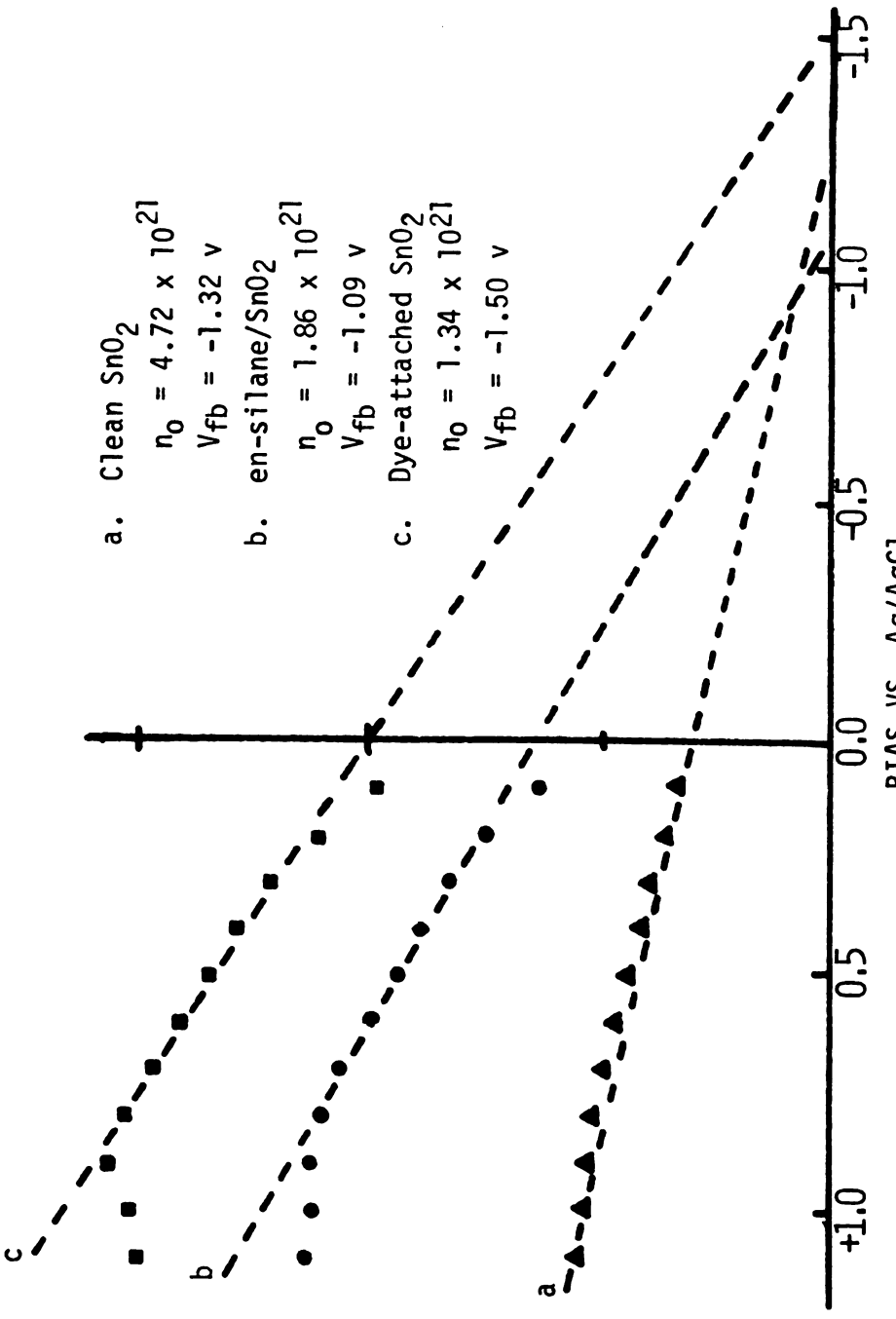

Figure 32. Mott-Schottky plot for Amide attached dye on en-silane modified SnO_2.

(electrochemical) dye assemblies. A goal of this research has been to compare the relative abilities of these two types of dye-modified surfaces to produce photocurrent. In this way, we may gain some insight into how critical covalent attachment is.

Figure 33 shows a plot of number of equivalent monolayers against photocurrent output. The photocurrents were measured at +1.0 volts, in pH 4 buffer oxalate solution (0.1 M). Filters used were an IR, LP 39 and BP 52 so that wavelengths between 425 and 625 were isolated, with a maximum transmittance occurring at 520 nm. Incident light was chopped at thirteen Hertz. The approximate number of monolayers for the electrochemical adsorption case were calculated as mentioned earlier. For the covalent case, one monolayer of dye was assumed, which may not be the case for the amide-attached route.

The most important effect to notice is that, in any given instance, the covalent attachment is always more efficient than the electrochemical adsorption per monolayer of material. Three distinct regions in the Figure are apparent. In region I, an increase in adsorbed monolayers has only a slight effect on the photocurrent production. At about 25 equivalent monolayers, the photocurrent output increases to a maximum (region II), and abruptly decreases (region III).

The decrease in photocurrent at higher coverages is expected. Gerisher (47) has observed that the quantum

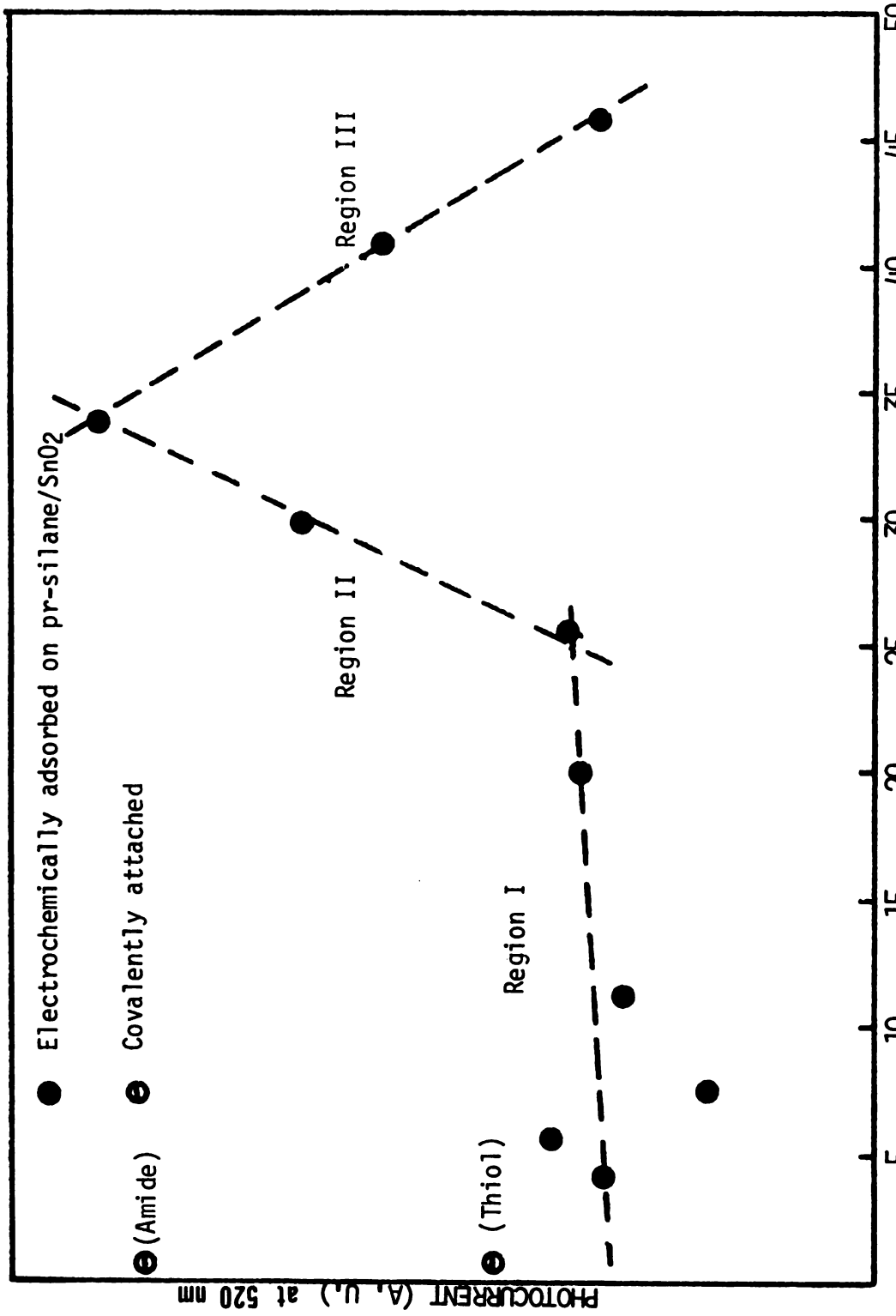

Figure 33. Photocurrent vs. monolayers for electrochemically adsorbed and covalently attached dyes (at 1.0 volts anodic).

efficiency for this type of configuration is limited by the fact that only monolayers of dye are active for electron transfer to the semiconductor in the excited state. Thicker layers only increase the resistance of the system without adding to the current generation. We have observed a similar phenomenon. The fact that the maximum in photocurrent occurs at such a high number of equivalent monolayers is not particularly disturbing, since we have no way of knowing that all the electrochemically adsorbed dye layers, as calculated from charge passed, are remaining on the surface.

This Figure, however, does indicate the importance of the covalent bond in electron transfer from the excited state of the dye to the semiconductor. Murrary (64,66) has suggested that the covalent linkage may allow the dye molecule to bend over in order to obtain the most efficiency for electron transfer. This plot indicates that the covalent linkage plays more than a passive role in the photocurrent process by allowing the dye more freedom to assume the most efficient orientation for electron transfer.

The fact that the photocurrent for the electrochemically adsorbed case reaches a maximum at such a high number of monolayers suggests that the adsorbed dye may reach an optimum surface concentration resulting in favorable overlap of the pi electrons of the dye and enhanced photocurrent activity.

F. Conclusion -- Suggestion for Future Work

The work presented is a major contribution towards the synthesis and characterization of modified electrode surfaces for photocurrent generation. In one case, that of the thiol, the covalent attachment plays a significant role in dye retention at the electrode surface. In the other case, amidization, proof of covalent attachment is insufficient, and we cannot be certain that an adsorption phenomenon is not occurring instead of the proposed attachment.

The multilayer electrochemical adsorption, which may also be producing a covalent linkage, also provides some interesting information on electrode modification.

The comparison of these two separate pathways in terms of their ability to effect photocurrent production at the semiconductor indicates the importance of the covalent linkage in photocurrent generation.

This research leaves several questions unanswered, however. Experimental work aimed at better characterization of the electrochemical adsorption process would be of importance, since it would answer the question of whether or not dye adsorption produces true covalent attachment. Such research would deeply involve such new techniques as ESCA and photoacoustic spectroscopy.

Further, the synthesis of multilayer covalently attached dye, not only erythrosin, would be of particular importance, based on the observations for the photocurrent efficiency for monolayers constructed by covalent attachment.

LIST OF REFERENCES

LIST OF REFERENCES

1. H. Horisaki, M. Hariya, K. Yazawa, Appl. Phys. Lett., 30,7 (1977).

2. H. Tributsch, H. Gerisher, Ber. Bunsenges. Phys. Chem., 73, 850 (1969).

3. T. Watanabe, A. Fujishima, O. Tatsuoki, K. Honda, Bull. Chem. Soc. Japan, 49, 8 (1976).

4. H. Kim, H. A. Laitinen, J. Electrochem. Soc., 122, 53 (1975).

5. R. Memming, G. Kursten, Ber. Bunsenges. Phys. Chem., 76, 4 (1972).

6. H. Gerisher, Photochem. and Photobiol., 16, 243 (1972).

7. H. Gerisher, F. Willig, Topics Current Chem., 61, 31 (1976).

8. T. Kuwana, R. K. Darlington, D. W. Leedy, Anal. Chem., 36, 2023 (1964).

9. W. N. Hansen, T. Kuwana, R. A. Osteryoung, ibid., 38, 1810 (1966).

10. D. Elliot, D. L. Zellmer, H. A. Laitinen, J. Electrochem. Soc., 117, 1343 (1970).

11. F. Mollers, R. Memming, Ber. Bunsenges, Phys. Chem., 76, 469 (1972).

12. N. R. Armstrong, A. W. C. Lin, M. Fujihira, T. Kuwana, Anal. Chem., 48, 741 (1976).

13. M. Babai, N. Tshernikovski, E. Gileadi, J. Electrochem. Soc., 119, 1018 (1972).

14. R. DeGryse, W. P. Gomez, F. Cardon, J. Vennik, J. Electrochem. Soc., 122, 711 (1975).

15. E. G. Gagnon, J. Electrochem. Soc., 121,512 (1974).

16. W. Mehl, F. Lohmann, Electrochim. Acta., 13, 1459 (1968).

17. H. A. Laitinen, C. A. Vincent, T. M. Bednarski, J. Electrochem. Soc., 115, 1024 (1968).

18. J. J. Kirkland, J. J. DeStefano, J. Chromatog. Sci., 8, 309 (1970).

19. J. J. Kirkland, J. J. DeStefano, ibid., 12, 337 (1974).

20. W. A. Aue, G. R. Hastings, J. Chromatog., 42, 312 (1969).

21. D. C. Locke, J. Chromatog. Sci., 11, 120 (1973).

22. K. G. Allum, R. D. Hancock, I. V. Howell, S. McKenzie, R. C. Pitkethly, P. J. Robinson, J. Organomet. Chem., 87, 203 (1975).

23. Petrarch Catalog, Petrarch Chemicals, Levittown, PA.

24. P. R. Moses, L. Wier, R. W. Murray, Anal. Chem., 47, 1882 (1975).

25. E. Grushka, Ed., "Bonded Stationary Phases in Chromatography," Ann Arbor Science Pub., Ann Arbor, MI.

26. C. R. Hastings, W. A. Aue, J. M. Augl, J. Chromatog., 53, 506 (1970).

27. P. G. Harrison, E. W. Thornton, J.C.S. Faraday I, 72, 1310 (1976).

28. P. G. Harrison, E. W. Thornton, ibid., 72, 1317 (1976).

29. C. M. Elliott, R. W. Murray, Anal. Chem., 48, 1247 (1976).

30. Corning Biomedical Supports, Pierce Chemical Company, Rockford, IL., 61105.

31. P. Edman, Acta. Chem. Scand., 4, 283 (1950).

32. R. A. Laursen, Eur. J. Biochem., 20, 89 (1971).

33. E. Wachter, W. Machleidt, H. Hofner, J. Otto, FEBS Letters, 35, 97 (1973).

34. G. B. Harper, Anal. Chem., 47, 246 (1975).

35. P. R. Moses, R. W. Murray, J. Electrochem. Soc., 77, 393 (1977).

36. J. R. Lenhard, R. W. Murray, J. Electron. Chem., 78, 195 (1977).

37. B. F. Watkins, J. B. Behling, E. Kariv, L. L. Miller, JACS, 97, 3549 (1975).

38. B. F. Firth, L. L. Miller, M. Mitani, T. Rogers, J. Lennox, R. W. Murray, JACS, 98, 8271 (1976).

39. M. Fujihira, T. Matsui, T. Osa, Chem. Lett., 875 (1976).

40. M. Fujihira, Nature, 264, 349 (1976).

41. P. R. Hammond, A. N. Fletcher, D. E. Bliss, R. A. Henry, R. L. Atkins, D. W. Moore, Appl. Phys. Lett., 9, 67 (1976).

42. L. N. Ionov, I. A. Akimov, Pis'ma Zh. Tekh. Fiz., 1, 881 (1975).

43. V. Lebedev, Khim. Zhizn, 9, 85 (1973).

44. M. M. Martin, L. Lindquist, J. Luminesc., 10, 381 (1975).

45. B. G. Harper, U. S. Patent 3904373 (Oct. 25, 1973).

46. H. Tributsch, M. Calvin, Photochem. and Photobiol., 14, 95 (1971).

47. H. Gerischer, Electroanal. Chem., 58, 263 (1975).

48. B. E. Conway, H. Angerstein-Kojlowska, W. B. A. Sharp, Z. Phys. Chem., 98, 61 (1975).

49. L. Balsene, H. Berthou, C. K. Jorgensen, Chimia, 29, 64 (1975).

50. I. M. Chaiken, E. L. Smith, J. Biol. Chem., 244, 5096 (1969).

51. B. B. Hasinoff, Can. J. Biochem., 49, 742 (1971).

52. O. R. Brown, Electrochemistry, 5, 220 (1975).

53. A. Laurent, E. Laurent, R. Tardival, Tetrahedron Lett., 4861 (1973).

54. L. L. Miller, A. K. Hoffman, JACS, 89, 593 (1967).

55. J. H. Scofield, J. Electron Spectrosc., 8, 129 (1976).

56. R. N. Adams, "Electrochemistry at Solid Electrodes," Marcel Dekker, New York (1969).

57. M. Gratzel, K. M. Bansal, A. Henglein, Ber. Bunsenges. Phys. Chem., 77, 11 (1973).

58. C. Birr, Justus Liebigs. Ann. Chem., 729, 213 (1969).

59. R. Paul, G. W. Anderson, JACS, 82, 4596 (1960).

60. N. F. Albertson, Organic Reactions, 12, 205 (1962).

61. D. F. Mironova, Uka. Khim. Zh., 35, 726 (1969).

62. A. Vijh, Electrochemistry of Metals and Semiconductors, Marcel Dekker, New York (1973).

63. S. S. Fratoni, S. P. Perone, Anal. Chem., 48, 287 (1976).

64. D. F. Untereker, J. C. Lennox, L. M. Wier, P. R. Moses, R. W. Murray, J. Electroan. Chem., (in press).

65. L. T. Minnis, M. A. McKnight, R. W. Murray, Anal. Chim. Acta, 89, 355 (1977).

66. J. C. Lennox, R. W. Murray, J. Electroan. Chem., 78, 395 (1977).

67. D. G. Davis, R. W. Murray, Anal. Chem., 49, 194 (1977).

68. K. Siegbahn, C. Nordling, A. Fahlman, R. Nordberg, K. Hamrin, J. Hedman, G. Johansson, T. Bergmark, S. Karlsson, I. Lindgren, B. J. Lindberg, "ESCA Atomic and Molecular and Solid State Structure Studies by Means of Electron Spectroscopy," Almquist and Wiksells, Uppsala (1967).

69. K. Siegbahn, C. Nordling, G. Johansson, J. Hedman, P. F. Heden, K. Hamrin, U. Geluis, T. Bergmark, L. Werme, R. Manne, Y. Baer, "ESCA Applied to Free Molecules," North Holland-American Elsevier, Amsterdam, New York (1969).

70. T. A. Carlson, G. E. McGuin, J. Electron Spectrosc., 1, 161 (1972/73).

71. P. W. Palmberg, Anal. Chem., 45, 549A (1973).

72. A. W. C. Lin, N. R. Armstrong, T. Kuwana, Anal. Chem., 49, 1228 (1977), and references therein.

73. E. Gileadi, E. Kirowa-Eisner, I. Pencinea, "Interfacial Electrochemistry," Addison-Wesley, London (1975).

74. A. Arai, U. S. Patent 3871879 (March 18, 1975).

75. N. R. Armstrong, C. N. Sayers, personal communication, Michigan State University, East Lansing, MI.

76. H. Gerisher, J. Electrochem. Soc., 113, 1174 (1966).

77. H. Gerisher, H. Tributsch, Ber. Bunsenges Phys. Chem., 72, 437 (1968).